NASA CR-159754

DISTORTION ANALYSIS FOR F100(3) ENGINE

JANUARY 1980

By W. A. Walter and M. Shaw

UNITED TECHNOLOGIES CORPORATION
PRATT & WHITNEY AIRCRAFT GROUP
GOVERNMENT PRODUCTS DIVISION

Prepared for
National Aeronautics and Space Administration

NASA Lewis Research Center
Contract NAS3-20335

FOREWORD

This report was prepared for the National Aeronautics and Space Administration, Lewis Research Center, under Contract NAS3-20835. The report documents the analysis of F100(3) compression system response to inlet circumferential distortion using the P&WA multiple segment parallel compressor model. Mr. H. George Hurrell was the NASA Project Manager with Mr. W. M. Braithewaite providing technical direction. Mr. W. J. Deskin was the P&WA Program Manager with Mr. W. A. Walter providing technical management assisted by Mr. M. Shaw. Mr. R. S. Mazzwy of P&WA's Commercial Products Division acted as a consultant for this program.

TABLE OF CONTENTS

LIST OF ILLUSTRATIONS

LIST OF ILLUSTRATIONS (Continued)

LIST OF ILLUSTRATIONS (Continued)

LIST OF TABLES

SUMMARY

This report documents the results of a study to evaluate the effect of individual and combined circumferential pressure and temperature distortions on F100(3) engine stability. The objective of this program was to analytically predict F100(3) response to these distortions using the Pratt & Whitney Aircraft Multiple Segment Parallel Compressor Model. Predicted F100(3) distortion response characteristics, together with past engine test experience, were then used to determine the distortion amplitudes required to stall F100(3) engine XD11 and plan future F100(3) distortion tests with this engine at NASA Lewis Research Center.

Study results showed that turbofan compression system response to combined pressure and temperature distortion depends upon the relative orientation, as well as the individual amplitudes and circumferential extents of the distortions. The study also showed the usefulness of the analytical predictions in planning engine and rig distortion tests, which includes better definition of instrumentation locations and distortion variations needed to establish engine compression system response characteristics.

INTRODUCTION

The operational suitability of an aircraft propulsion system depends on engine response to inlet pressure and/or temperature distortions. These distortions may result in reduced system stability or a complete loss of stable system operation. Definition of engine response to distortion and assurance of adequate engine stability margin usually requires that extensive testing be conducted. To improve and reduce the amount of experimental stability testing, Pratt & Whitney Aircraft and the NASA Lewis Research Center (NASA LeRC) collaborated in developing an analytical model which predicts engine response to circumferential pressure, temperature, and combined pressure and temperature distortion. Extensive work was accomplished in predicting the response characteristics of a turbofan engine with nonvariable compressor geometry (TF30) under NASA Contract NAS3-18535. NASA Contract NAS3-20010 then expanded the distortion model to include variable fan and compressor geometry effects. The work reported herein utilized this expanded model to predict the distortion response characteristics of the F100(3) engine. In addition, these predictions were used to ascertain the levels of distortion required to stall F100(3) engine XD11-8 as part of a pretest planning effort, thus demonstrating the usefulness of the model predictions in designing improved engine stability tests.

This program consisted of three technical tasks. Task I evaluated the effect of individual circumferential pressure and temperature distortions on F100(3) engine stability. Distortion amplitude and circumferential extent effects were established using the Pratt & Whitney Aircraft Multiple Segment Parallel Compressor Model and compared to existing F100(3) pressure distortion characreristics. In Task II, the distortion analysis was expanded to include combined pressure and temperature distortion effects. Predicted engine response to combined distortion was compared to the Task I individual distortion response characteristics. An approach was defined using this comparison to predict the combined effects from uncombined distortion test results. Finally, in Task III the predicted distortion response characteristics were used to determine the levels of individual and combined distortion required to stall F100(3) engine XD11-8.

ENGINE DESCRIPTION

The F100(3) is an advanced, twin-spool, augmented turbofan engine currently operating in both the F-15 and F-16 aircraft. The engine compression system consists of a three-stage fan and 10-stage high-pressure compressor. Variable vanes are incorporated in both the fan and compressor. Fan inlet guide vane angle is scheduled as a function of low spool rotor speed corrected to the fan inlet temperature. The compressor variable vanes are scheduled as a function of high rotor speed corrected to the fan exit bypass stream temperature. The variable vane sensor locations are shown schematically in figure 1. From the figure it can be inferred that the relative orientation of the inlet distortion will affect the engine's response due to rescheduling of the variable vane rows.

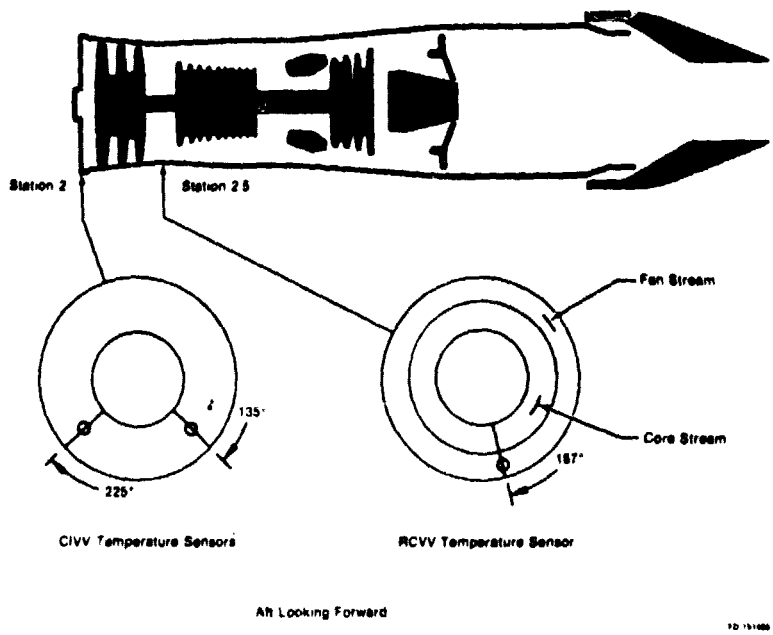

Figure 1. Temperature Sensor Locations for F100(3) Variable Vane Control

DISTORTION MODEL DESCRIPTION

The following is a brief overview of the distortion model used in predicting engine and compression system distortion response characteristics. A more detailed description of the model is presented in References 1 and 2.

The Pratt & Whitney Aircraft analytical distortion model uses an expanded parallel compressor theory to predict response to circumferential distortion. Multiple parallel compressor segments are used to provide a detailed definition of the circumferential flow field. Individual blade and vane row static pressure and total temperature rise characteristics are used to describe the compression system undistorted operating performance. Individual segment performance is adjusted to account for two-dimensional and unsteady flow effects which are not considered in basic parallel compressor theory. This includes the effect of engine-induced inlet flow redistribution, circumferential crossflows caused by internal compressor cavities, and unsteady flow due to rotor movement through a distorted flow field. Performance variations due to variable geometry are accounted for and include the effect on the swirl of the flow distortion pattern and

a fluid particle as they progress through the machine from inlet to exit. Individual compressor components and dual-spool fan/compressor configurations can be evaluated using the model.

ANALYSIS PROCEDURE

1. General

F100(3) circumferential distortion response characteristics were predicted using the Multiple Segment Parallel Compressor Flow Model. Eighteen (18) parallel compressor segments defined the circumferential flow field through both the fan and high-pressure compressor. For each distortion case, the fan bypass, fan core, and high-pressure compressor were independently evaluated. Evaluating engine distortion response characteristics at both 102 and 70% corrected fan rotor speed provided engine speed effects. Average engine inlet conditions (total pressure and temperature), assumed at 5.171×10^4 n/m^2 (7.5 psia) and 267.9°K (482.3°R), correspond with expected engine inlet conditions in future NASA LeRC F100(3) distortion tests.

2. Stall Criteria

Backpressuring both the fan bypass and core section until the maximum exit static pressure points were determined established the stall-limiting airflow rate. The backpressuring process was achieved by incrementally increasing the fan exit static pressure and attempting to find a continuous mass flow distribution that would satisfy this required pressure. As the required pressure increases, the average flowrate decreases, as shown in figure 2. An attempt to increase the pressure beyond the "stall point" results in a large redistribution of mass flow around the circumference, such that a continuous mass flow distribution cannot be found to satisfy this required pressure. For more detailed discussion, see reference 4.

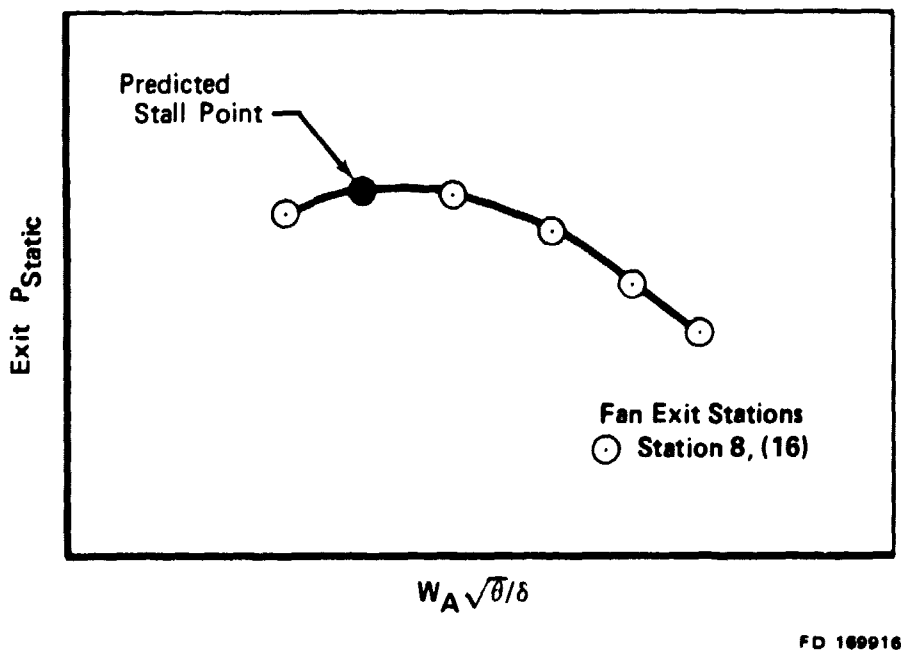

Figure 2. Stall Criteria: Max Static Pressure at Exit Station

3. Distortion Response Parameters

The determination of compression system response to distortion requires quantifying the magnitude of the inlet distortion and corresponding loss in surge pressure ratio. As a result, a distortion descriptor system is needed to quantify the distortion. In this study, both the F100(3) K# distortion descriptor system (see Appendix I) and the "classical" $\Delta P/\bar{P}$ max-min, $\Delta T/T$ max-min descriptors were used in the response analysis.

Several parameters were used to define the engine distortion response characteristics.

1. Component operating line rematch due to the applied inlet distortion — Defined in terms of the change in component average inlet corrected airflow and efficiency from the nominal undistorted to distorted operating points.

2. Stall line degradation of the limiting component — Defined as a function of the imposed distortion level. Surge margin loss was defined as the percentage difference between the mass average undistorted and distorted stall pressure ratio at the distorted stalling airflow rate.

3. Compression system attenuation/generation of pressure and temperature distortion across the core flow stream — Defined in terms of the levels of component exit distortion for each imposed inlet distortion and circumferential profiles of exit pressures and temperatures.

4. The distortion path through the stages of the engine compression system — Defined in terms of the row-by-row acoustic and particle flow angles. In addition, the circumferential pressure and temperature profiles were defined at the fan inlet, fan exit, and compressor exit stations.

4. Individual Distortion Analysis

Figure 3 shows the individual distortion patterns used to evaluate engine compression system stability characteristics. These cases include variations in distortion amplitude and circumferential extent. An orientation change was included in the temperature distortion cases (case 5 versus 7) to evaluate the effect of engine variable vane position on the distortion response. In addition, engine speed effects were evaluated by predicting engine response to the case 3 and 5 distortions at both 102 and 70% corrected fan rotor speed.

For each distortion case, the fan stall point was defined by increasing the fan backpressure, while holding the fan corrected speed and bypass ratio constant, until stall occurred. The high-pressure compressor was evaluated using the predicted fan exit core pressure and temperature distortions at the fan stall point. A constant exit static pressure boundary condition was assumed for both the fan and high-pressure compressor based on existing F100 test experience. Although this assumption was consistent with F100(3) experience, other engines may have a significant fan exit static pressure gradient due to the proximity of downstream compression components to the fan exit. Therefore, an evaluation of the effect of the exit static pressure profile on fan response characteristics was made.

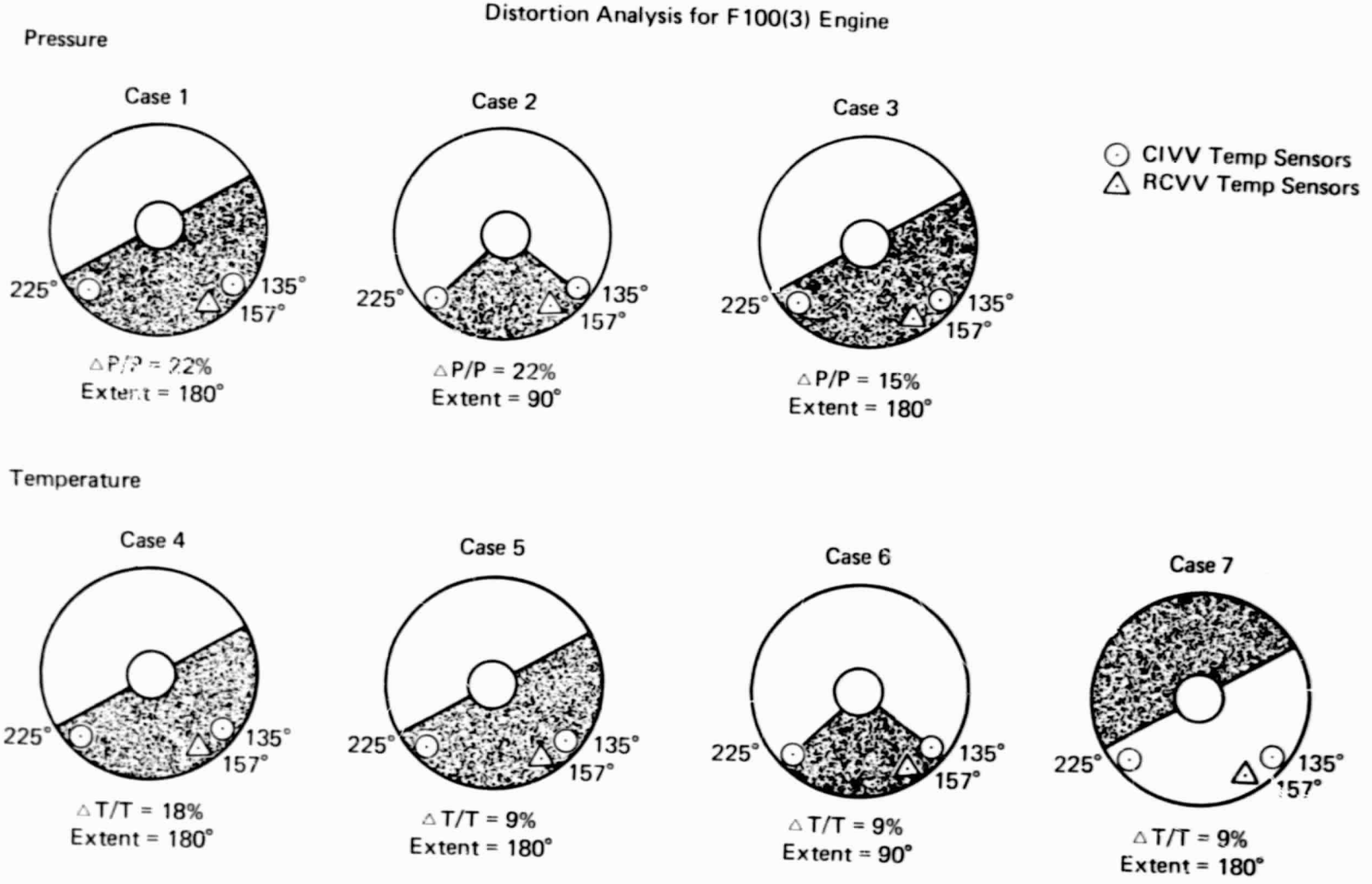

Figure 3. Task I Distortion Case

5. *Combined Distortion Analysis*

Previous analysis of engine operation with combined pressure and temperature distortion has shown that the engine response characteristics depend on the relative orientation of the distortions, as well as the amplitudes and circumferential extents of the distortions (see References 3 and 4). Figure 4 shows the five combined distortions used in this study to establish orientation effects. As with the individual distortion cases, the fan stall point was defined by increasing the fan backpressure until stall occurred. A constant static exit pressure boundary condition was assumed for both the fan and high-pressure compressor.

6. XD11-8 Stability Audit

The response characteristics defined for individual and combined distortions were used to predict the levels of distortion required to stall F100(3) engine XD11-8. Stall distortion levels were defined for each of the types of distortion analyzed under the individual and combined response tasks. The stall-limiting component was identified for each case. Results of the audits were used in planning future distortion tests with this engine. This included a definition of the required capability of the test pressure and temperature distortion generators as well as evaluating the need for engine rematch capability.

RESULTS AND DISCUSSION

INDIVIDUAL DISTORTION — SYSTEM ANALYSIS

1. Pressure Distortion

Compression system response to pressure distortion was predicted for the 102% speed condition using three different pressure patterns. Figure 5 shows the predicted fan surge points for these distortions. As would be expected, the 22% $\Delta P/P$, 180 deg distortion results in a lower surge line than the 15% $\Delta P/P$, 180 deg distortion. However, the 22% $\Delta P/P$, 90 deg distortion produced the lowest surge line.

Figures 6 and 7 show a comparison of model-predicted distortion sensitivity to the F100(3) stability correlation which is based on test data. Figure 6 shows this comparison using the F100(3) $K\theta$ distortion factor system, while Figure 7 presents the comparison in terms of the classical $\Delta P/P$ (max-min/avg) parameter. The F100(3) stability correlation levels shown in Figure 7 were established by converting the $K\theta$ correlation into an equivalent $\Delta P/P$. Separate correlation levels for 90 deg vs 180 deg distortions result since the $\Delta P/P$ system only accounts for the distortion level and not its angular extent.

As can be seen in Figure 6, the model predictions show reasonable agreement on a $K\theta$ basis with the F100(3) correlation, except for the Case 3 (15% $\Delta P/P$) point. The Case 1 and 2 predictions do indicate a higher fan sensitivity to 90 deg distortions than 180 deg distortions. This becomes even more evident in Figure 7 where the Case 2 point is much higher than the 90 deg correlation level.

As noted above, the Case 3 (15% $\Delta P/P$) point showed poor agreement with the F100 stability correlation. Therefore, the model-predicted profiles were compared to F100 test data to further evaluate this case. Figure 8 shows that the model-predicted exit total pressure profile compare to test data. The deviation of the predictions from the test data are due to differences in the inlet profiles, data accuracy, and model accuracy with this low level distortion case. Analysis of this case showed the need to test with reasonable levels of distortion and/or perform analytical studies with reasonable distortion levels to avoid inaccuracies in fan/compressor sensitivity parameters.

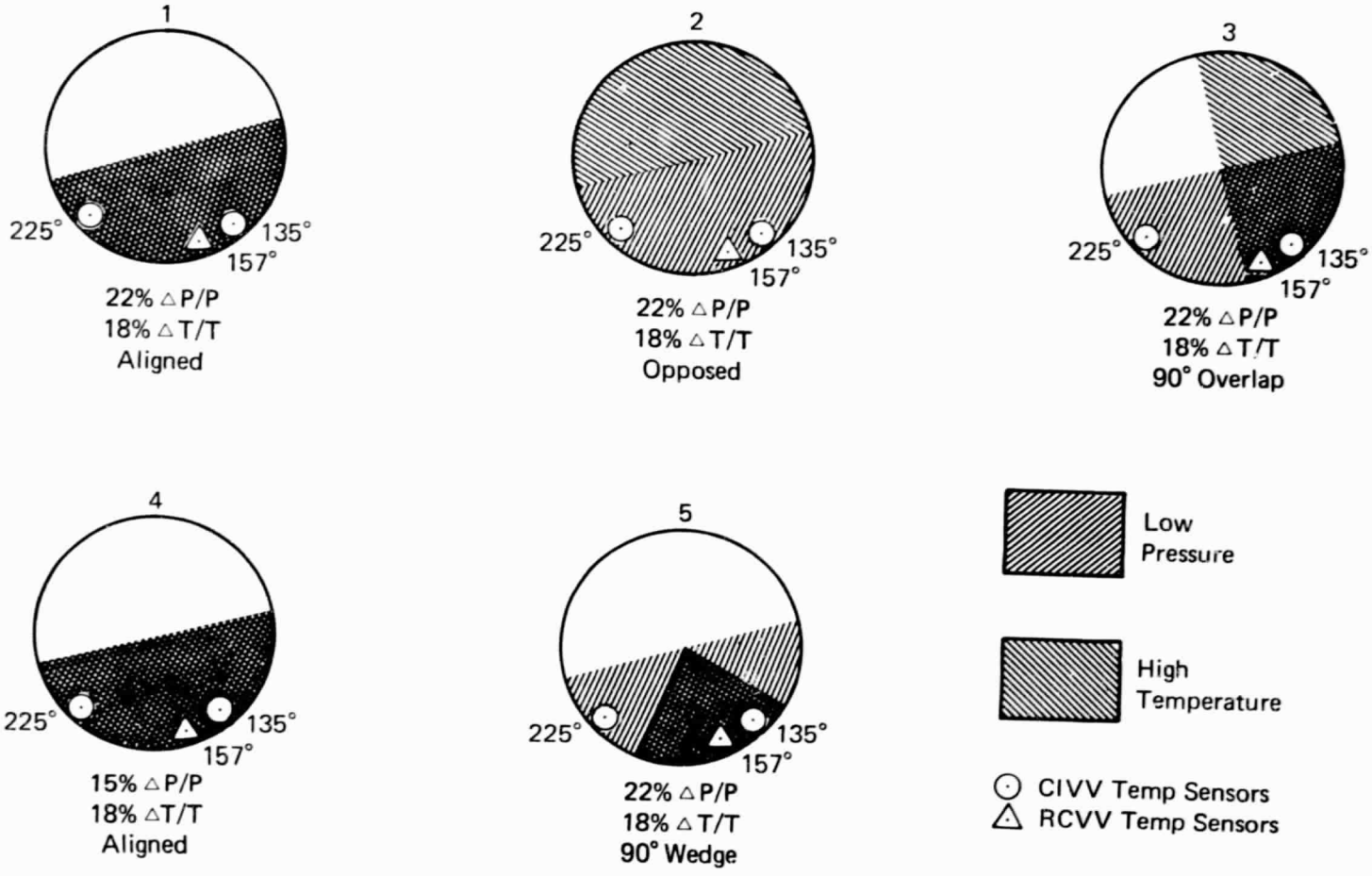

Figure 4. Combined Distortion Cases

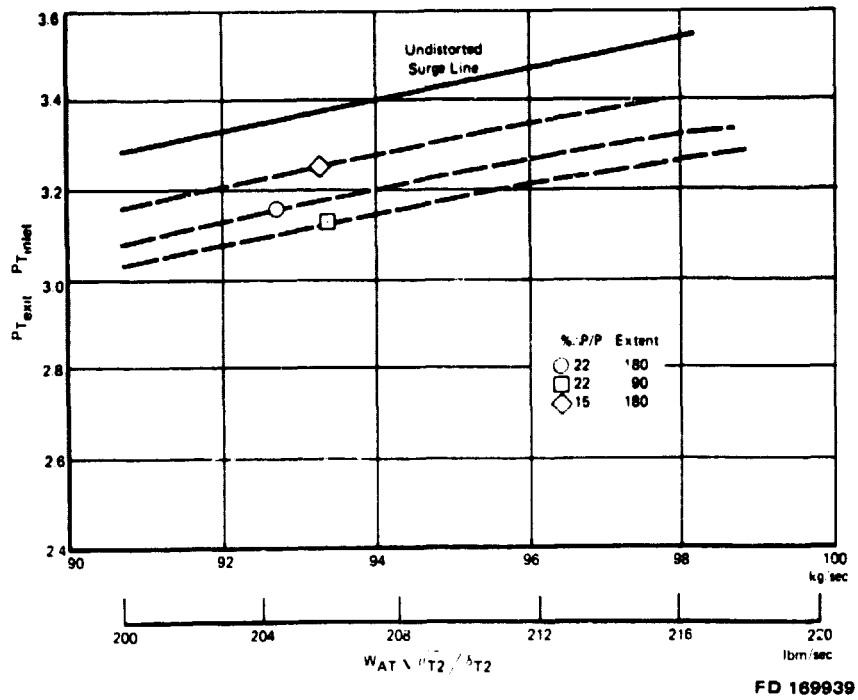

Figure 5. Predicted F100(3) Fan Surge Lines With Pressure Distortion

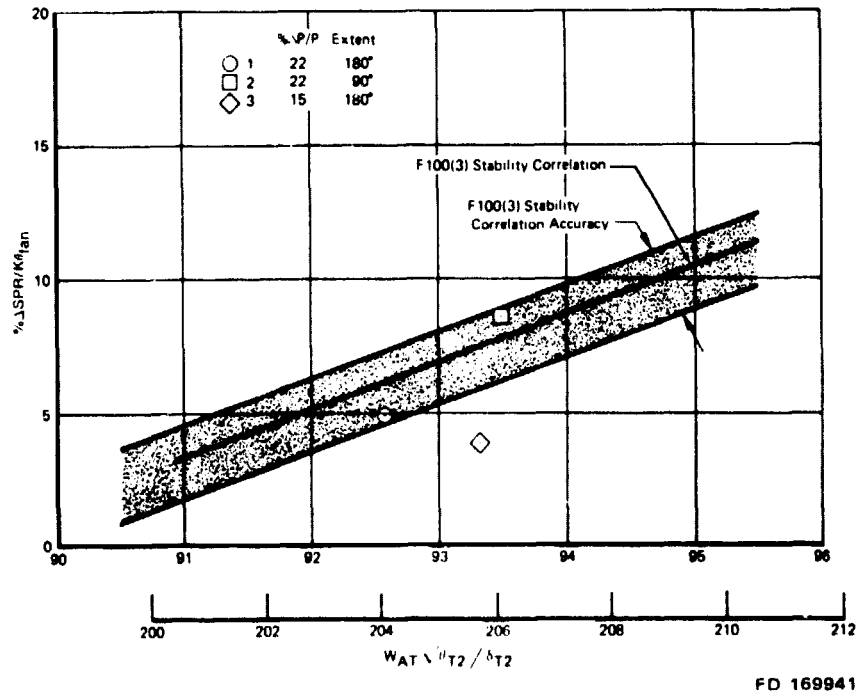

Figure 6. Circumferential Pressure Distortion Kθ Sensitivity

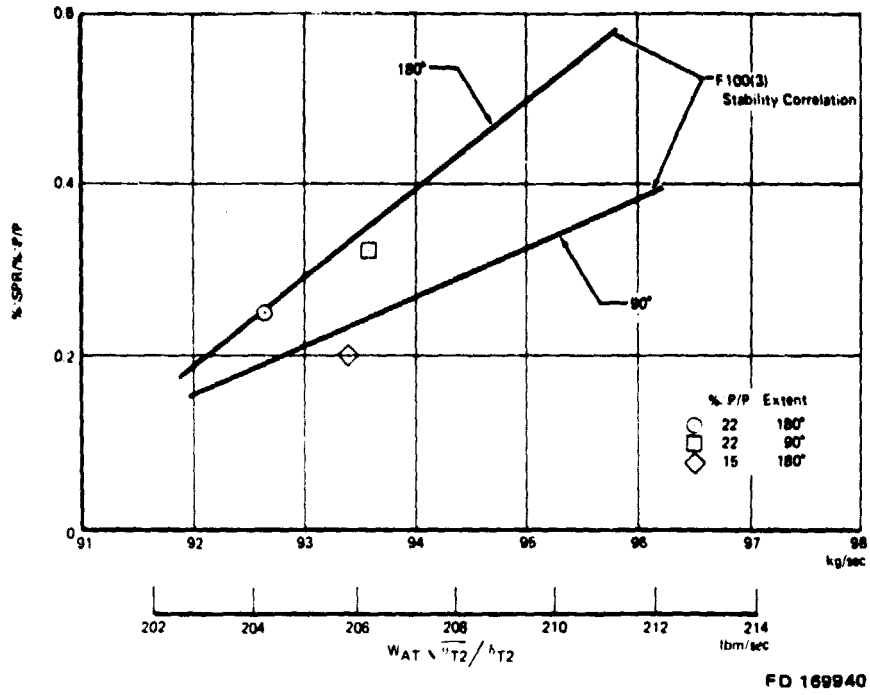

Figure 7. Circumferential Pressure Distortion ΔP/P Sensitivity

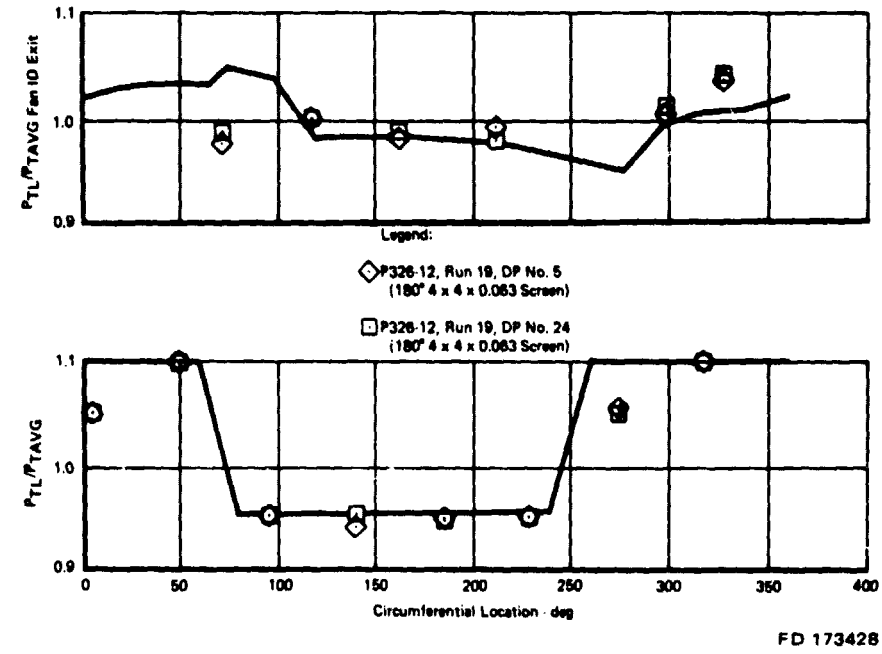

Figure 8. Comparison of F100(3) Engine Data and Predictions

The evaluation of overall engine operation with inlet distortion requires defining the distortion transfer characteristics of each compression system component. In the F100(3) engine, attenuation of inlet distortion through the fan results in an inlet temperature distortion at the high pressure compressor. Therefore, evaluation of the stability response of the high compressor requires definition of the level of pressure distortion remaining at the fan core stream exit and the level of generated temperature distortion at the high compressor inlet that results from attenuating the pressure distortion.

Figures 9 and 10 show the predicted fan core stream pressure distortion attenuation characteristics of the F100(3) fan. The predictions show that the fan significantly attenuates the inlet pressure distortion, thereby reducing the stability threat to the high pressure compressor. Although only predicted attenuation characteristics are shown on figures 9 and 10, F100(3) test data showed similar attenuation characteristics for 180 deg distortion.

However, the model predictions did show a different attenuation level with 90 deg vs 180 deg inlet distortion. Analysis of the attenuation characteristics using the F100(3) distortion descriptor system (as shown in figure 9) indicated less attenuation of the 90 deg distortion than the 180 deg distortions. Conversely, analysis using simple $\Delta P/P$ distortion descriptors showed the opposite: more attenuation of the 90 deg distortion, as shown in figure 10. This apparent inconsistency is due to a change in the circumferential extent of the 90 deg distortion at the fan exit vs fan inlet which is not reflected in the $\Delta P/P$ distortion descriptors. Figure 11 shows the circumferential pressure distribution at the fan inlet vs fan exit for the 90 deg distortion case. As can be seen, the exit distortion is lower in level, but 155 deg in extent. This extent change results in a KO at the fan exit that is higher than a case where only the level of distortion changed. The $\Delta P/P$ system only reflects the level change and therefore shows more attenuation than the KO system. However, past experience indicates that the KO system better reflects the engine response to distortion and therefore exit distortion characteristics based on this system are more representative of the threat to the high pressure compressor.

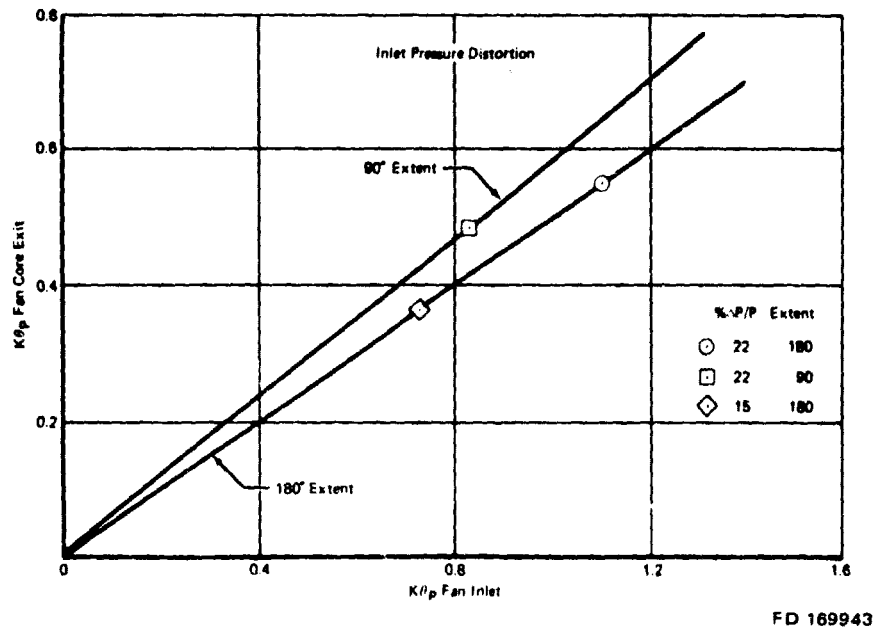

Figure 9. Predicted F100(3) Fan Distortion Attenuation: Kθ

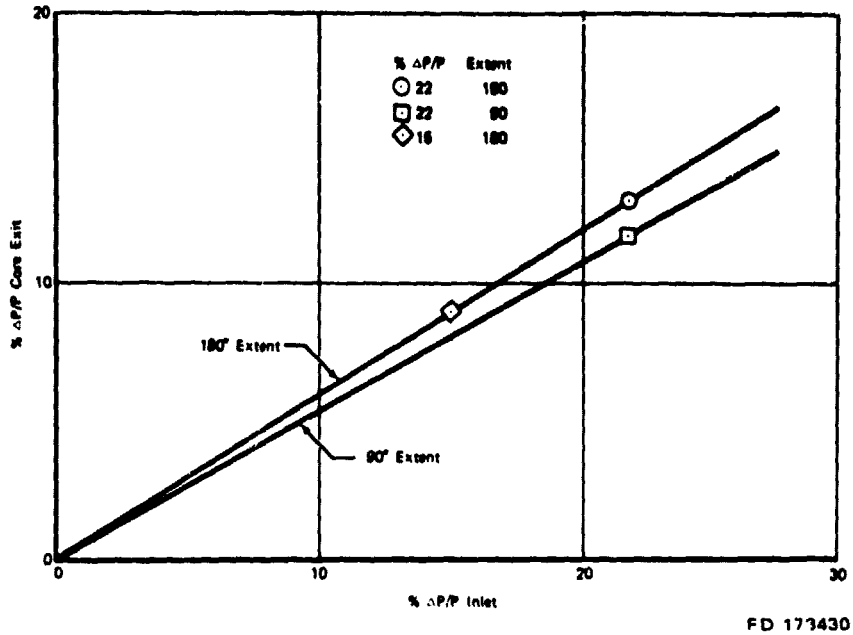

Figure 10. Predicted F100(3) Fan Distortion Attenuation: ΔP/P

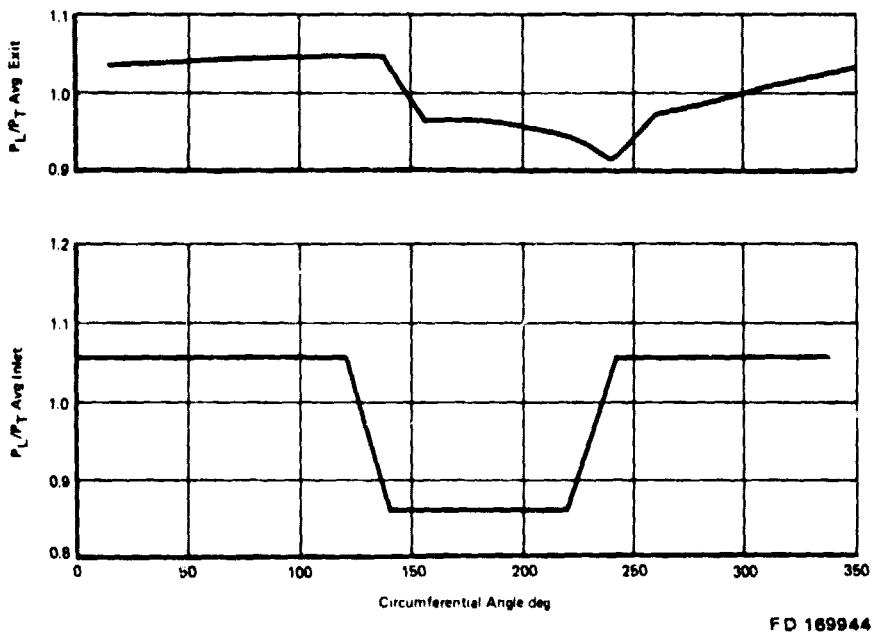

Figure 11. Predicted Angular Extent Change for 90 deg Distortion

The attenuation of pressure distortion by a compression component results in the generation of an exit temperature distortion. This is due to a difference in the work between the distorted vs undistorted region of the component needed to meet the exit pressure boundary condition. Figures 12 and 13 show the predicted F100(3) fan exit temperature distortion characteristics. Slightly more temperature distortion is predicted for the 90 deg distortion case.

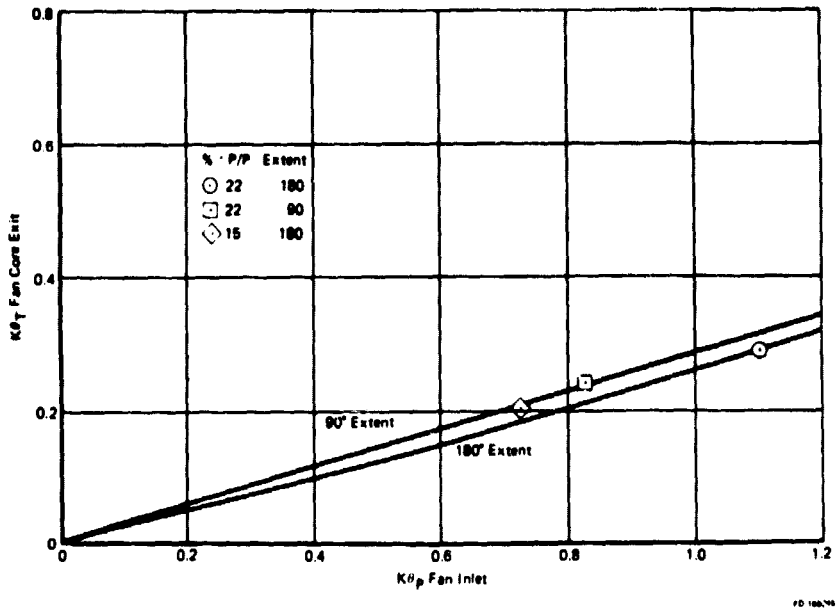

Figure 12. Predicted F100(3) Fan Temperature Distortion Generation: $K\theta_T$

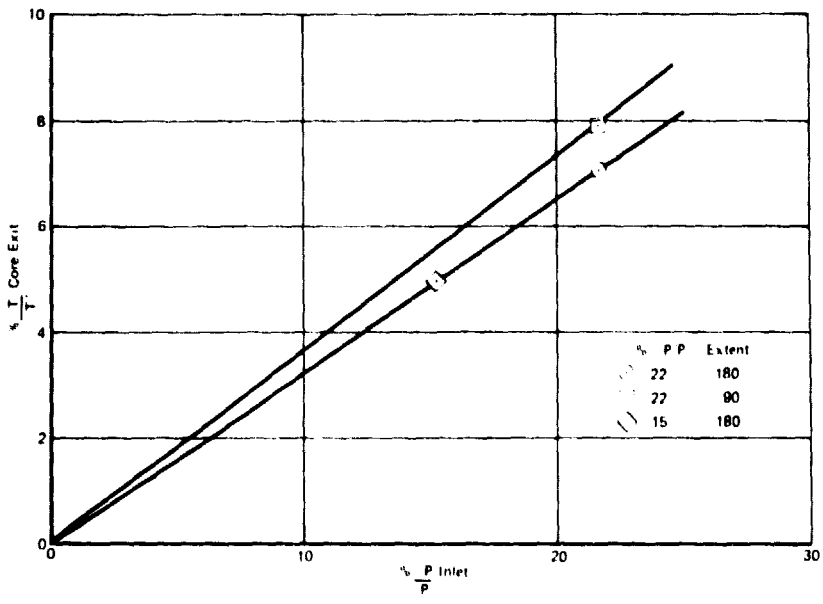

Figure 13. Predicted F100(3) Fan Temperature Distortion Generation: $\Delta T/T$

2. Temperature Distortion

Engine response to temperature distortion was predicted for the 102% speed condition using four temperature patterns. This included an evaluation of the effect on fan response of a change in the inlet guide vane angle caused by a change in temperature distortion orientation.

Figure 14 shows the predicted fan surge points with temperature distortion. The fan is predicted to be less sensitive to temperature distortion than pressure distortion, as can be seen in figures 15 and 16. Fan response to 90 deg temperature distortion was approximately the same as for 180 deg distortion. The scatter in the predicted temperature distortion sensitivities was felt to be due to model accuracy when predicting response to low levels of distortion (9% $\Delta T/T$). As a result, the temperature distortion level was set at 18% $\Delta T/T$ for combined distortion analysis to minimize scatter introduced by model accuracy.

The distortion transfer characteristics of the fan when operating with temperature distortion were also evaluated. Figures 17 and 18 show the level of fan core exit temperature distortion vs fan inlet temperature distortion. The fan is predicted to transmit almost all the temperature distortion to the high pressure compressor. No discernible difference was predicted between 90 deg vs 180 deg distortion attenuation characteristics.

The fan is also predicted to generate an exit total pressure distortion when operating with temperature distortion. This pressure distortion results from the fan operating at different corrected speeds and flow rates in the high temperature vs low temperature region of the distortion. Since the fan was assumed to have a constant exit static pressure, the varying flow rate caused by the temperature distortion results in an exit total pressure distortion. Figures 19 and 20 show that significant levels of exit pressure distortion are predicted to occur with temperature distortion.

The effect of temperature distortion orientation on fan response was evaluated. The orientation of the temperature distortion affects the temperature measurements used in scheduling the fan inlet guide vanes. A comparison of cases 5 and 7, which had different distortion orientations, shows that the predicted surge line less was affected by the distortion orientation. However, the fan distortion attenuation and pressure generation characteristics were approximately the same.

3. Distortion Rematch

The effect of inlet distortion on the fan match was evaluated as part of this program. Table 1 shows that the distortion had a small effect on fan match at high power which was consistent with test experience. Since this effect was small at high power with high distortion levels, no attempt was made to quantify the rematch with lower distortions and/or low power operation.

Table 1. Distortion Effect on Fan Match

Case	*Type*	*% $\Delta P/P$ or % $\Delta T/T$*	*ΔEfficiency*	*ΔFlow (kg/sec)*
1	Pressure	22	−0.94	0.39
4	Temperature	18	0.34	−0.005

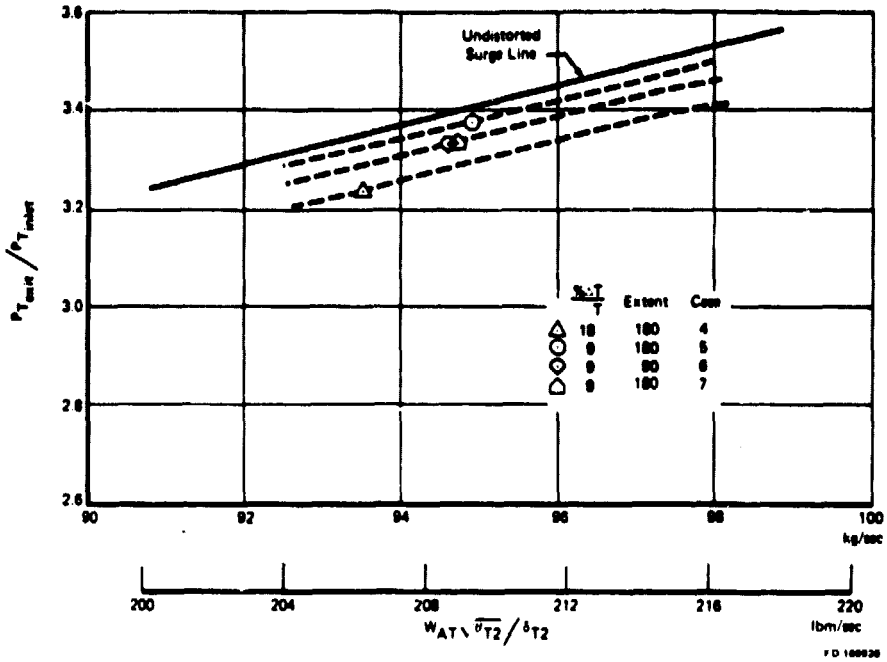

Figure 14. Predicted F100(3) Fan Surge Lines With Temperature Distortion

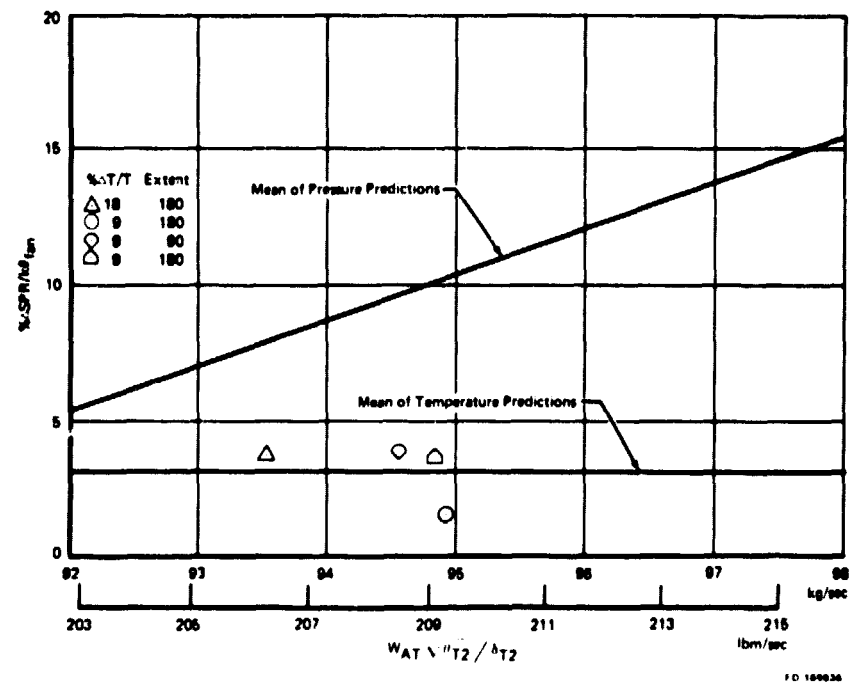

Figure 15. Response Comparison: Temperature vs Pressure Distortion ($K\theta_T$, $K\theta_P$)

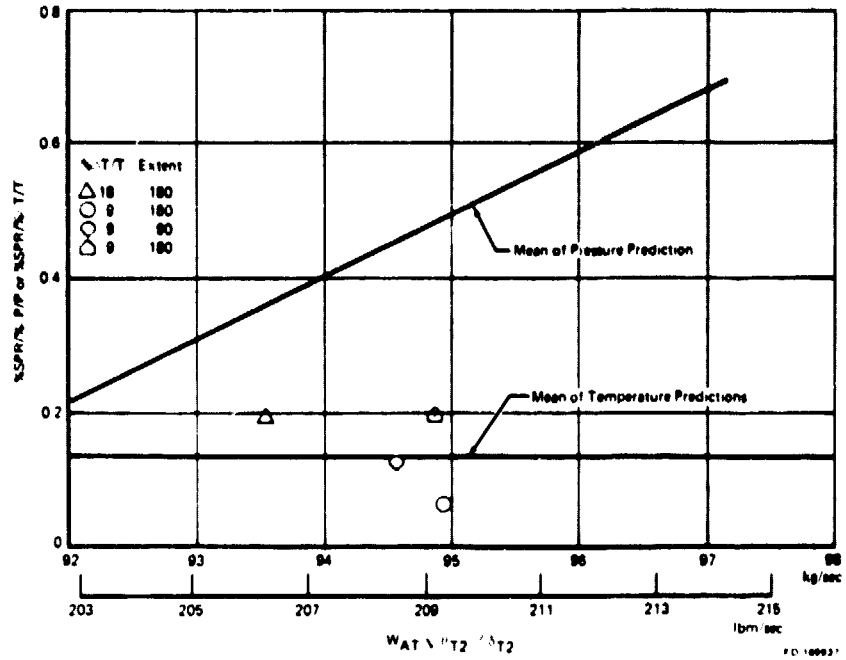

Figure 16. Response Comparison: Temperature vs Pressure Distortion ($\Delta T/T$, $\Delta P/P$)

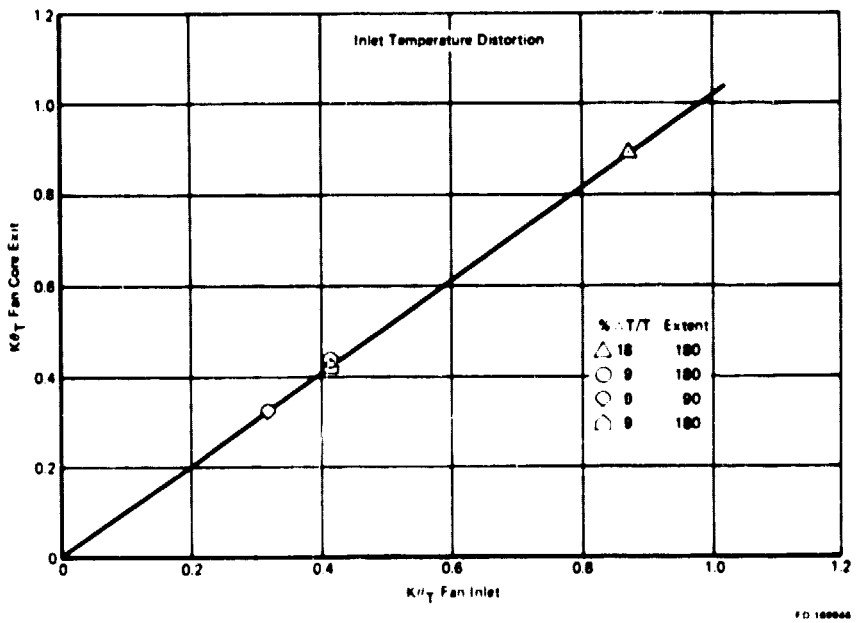

Figure 17. Predicted F100(3) Fan Temperature Distortion Attenuation: $K\theta_T$

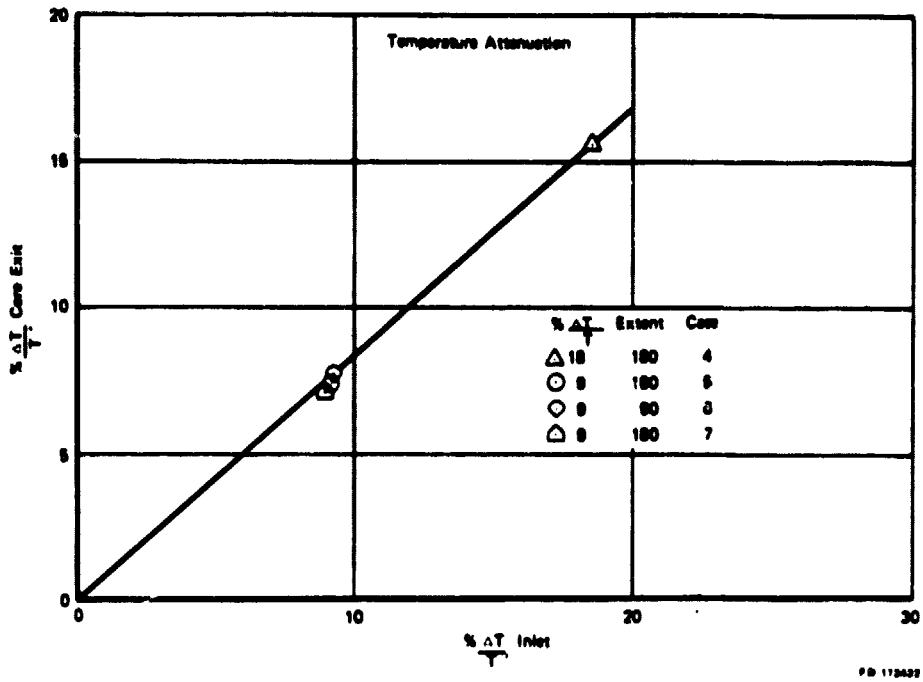

Figure 18. Predicted F100(3) Fan Temperature Distortion Attenuation: ΔT/T

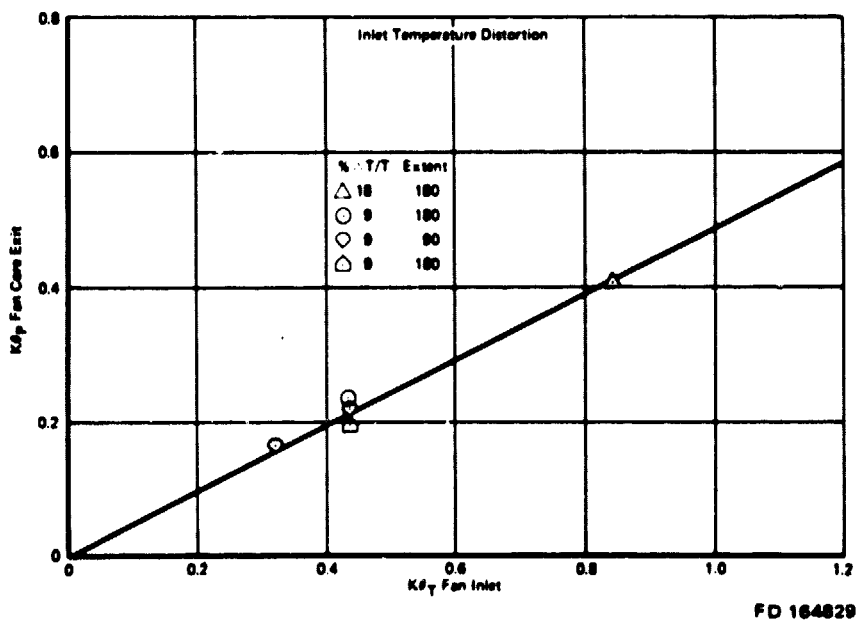

Figure 19. Predicted F100(3) Fan Pressure Distortion Generation: $K\theta_p$

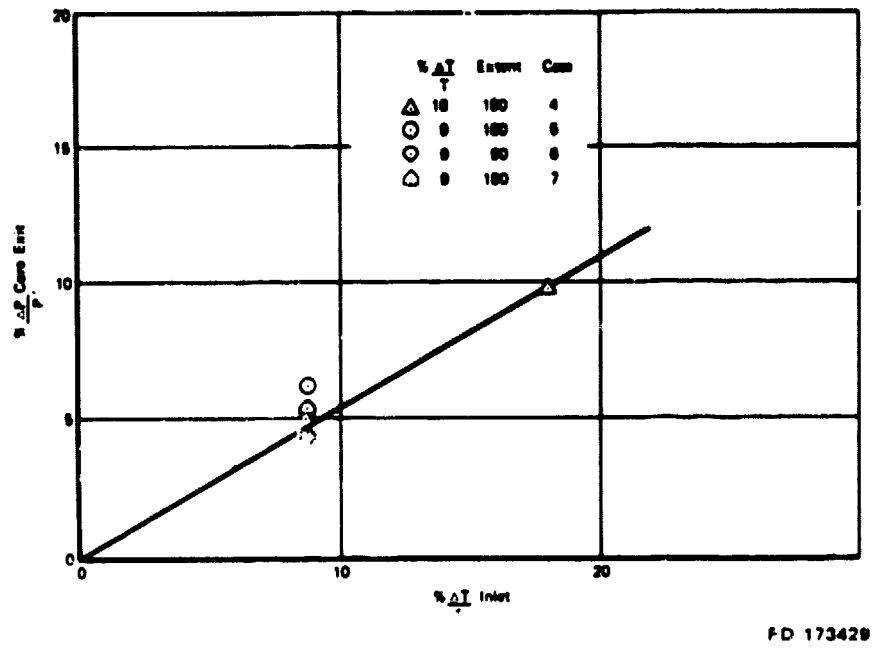

Figure 20. Predicted F100(3) Fan Pressure Distortion Generation: ΔP/P

4. Low Power Predictions

Engine speed effects were investigated by evaluating engine response to the case 3 and 5 distortions at both 102% and 70% corrected fan rotor speed. Figure 21 shows a comparison of model predicted fan distortion sensitivity to the F100(3) correlation at 70% corrected fan rotor speed. The model predicted fan pressure distortion sensitivity is significantly higher than the test data correlation. This discrepancy could be due to many factors, including the definition of the low power row characteristics, cross flow calculations, modeling of bypass ratio effects, extreme level of distortion for an Idle power condition, and flow mixing procedures in the model. Resolution of this problem was felt to be beyond the scope of the current program, but should be investigated in future efforts.

INDIVIDUAL DISTORTION — DETAILED FLOW FIELD ANALYSIS

The P&WA Multiple Segment Parallel Compressor Model provides both a row-by-row and major station definition of the flow field through the engine compression system. In modeling the F100(3) engine, the fan was divided into a core and bypass stream. Separate station designations were assigned to each row and stream through the fan and high pressure compressor. Figure 22 shows the station designations used in the F100(3) model.

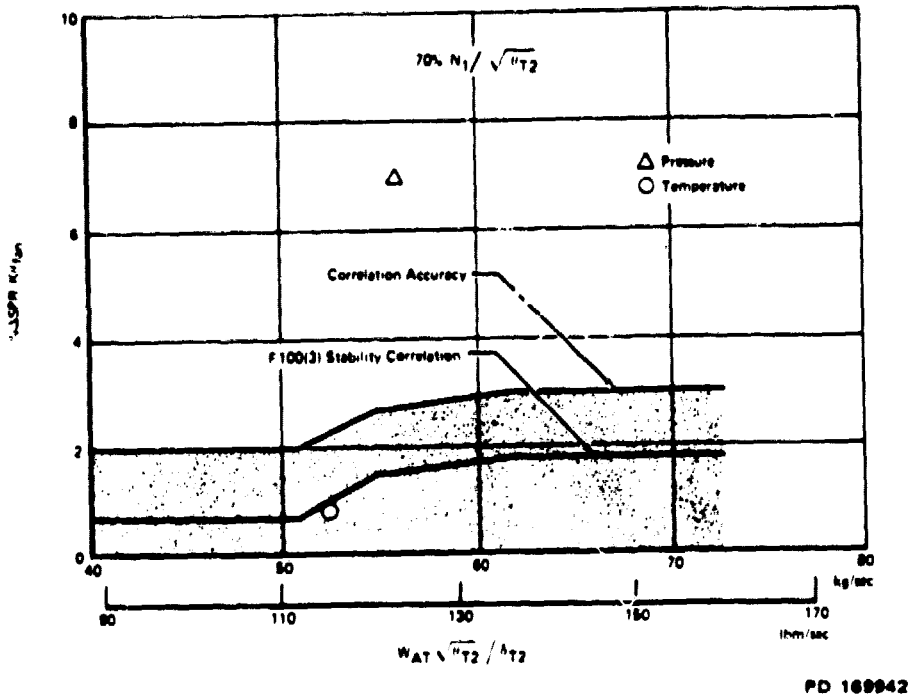

Figure 21. Low Power Distortion Sensitivity

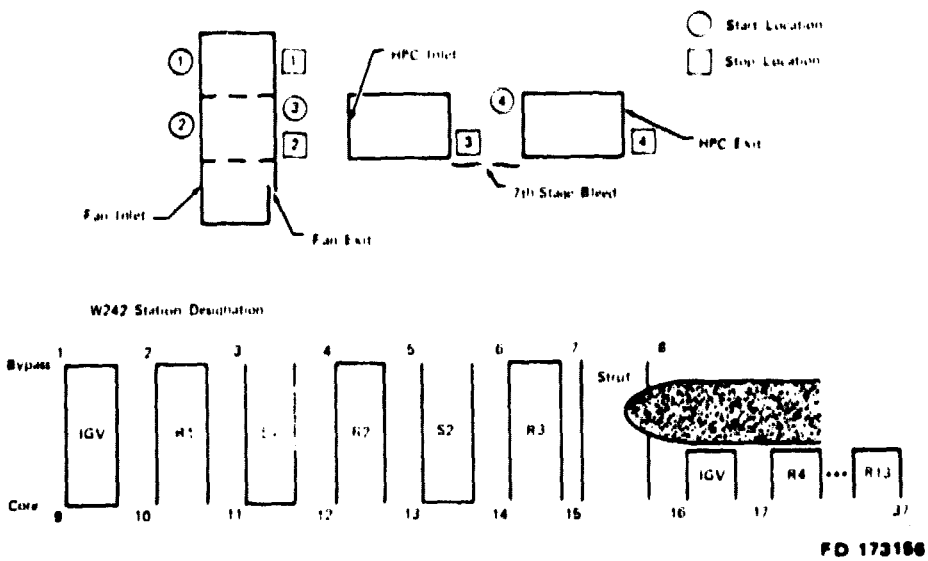

Figure 22. Model Station Designations

The flow field through the engine compression system was defined for both undistorted and distorted operation. In addition, the effect of fan operating level on the flow field was defined. Several parametric studies were also made to define the effect on engine response of (1) the assumed constant static pressure boundary condition, (2) level of engine bypass ratio and (3) the effect of model input values that alter iteration and/or stall point evaluation routines.

In the F100(3) engine, the distorted flow field characteristics of the fan core are of primary interest for two reasons: the stall line sensitivity of the fan is dependent upon the characteristics, and distortion at the high pressure compressor face is determined by these characteristics. The individual particle and acoustic paths through the core compression system are shown in figure 23 for undistorted operation at 102% corrected fan rotor speed. The paths are shown for both a near stall and nominal operating point. Through the fan core a particle is predicted to swirl approximately 65 deg while the faster traveling acoustic signal (flow swirl) is translated approximately 35 deg.

The swirl through the machine is primarily set by rotor speed and blade/vane geometry. Figure 24 shows that the variation in flow and particle swirl of the distorted cases from the undistorted case is small. (A complete tabulation of these variations is also provided in table 2.) Therefore, in designing an instrumentation scheme for distortion testing, it should be sufficient to estimate these paths for undistorted operation and use them for locating distortion probes and rakes.

Fan core exit pressure and temperature profiles for individual 180 deg extent, inlet pressure and temperature distortion cases are presented in figure 25. In both cases, significant overlapping of the low pressure and high temperature regions exists at the high pressure compressor (HPC) inlet. As will be shown in the combined distortion analysis, this alignment of the low pressure and high temperature distortion at the fan exit results in the "worst" possible case for the HPC.

Figures 26 through 35 show representative pressure and temperature profiles at major engine stations for the high pressure and temperature distortion cases. Also included on these figures are the exact flow and particle swirl angles predicted for each station.

As previously noted, a constant fan exit static pressure boundary condition was assumed in predicting F100(3) fan distortion response characteristics. Although this assumption was consistent with F100(3) experience, other engines may have a significant fan exit static pressure gradient due to the proximity of downstream compression components to the fan exit. Therefore, an evaluation of the exit static pressure profile effect on fan response characteristics was made. Figure 36 shows a comparison of the case 1 ($\Delta P/P$ 22%) fan exit profiles for a constant fan core exit static pressure vs a distorted fan core exit static pressure profile. This distorted profile is the one predicted to exist by the model when it is assumed the fan and high compressor are aerodynamically coupled. The constant fan exit static pressure boundary condition results in less fan exit total pressure distortion. In addition, the fan surge line loss with the constant fan exit static pressure boundary was double the loss with the exit static pressure profile. Classically, fan rig tests are conducted with a constant exit static pressure. This study shows that significant differences in response characteristics could result between the engine and rig if a fan exit static pressure profile exists in the engine. Fan rig distortion tests should include simulating the exit static pressure field measured in the engine. In addition, Reference 5 has shown that the response of a compressor to an inlet pressure distortion can be dependent upon downstream components.

During the evaluation of F100(3) response to individual distortion, several required inputs to the prediction model were varied to determine their impact on the stall predictions. These included variations in input bypass ratio, incremental exit static pressure step size and number of circumferential segments.

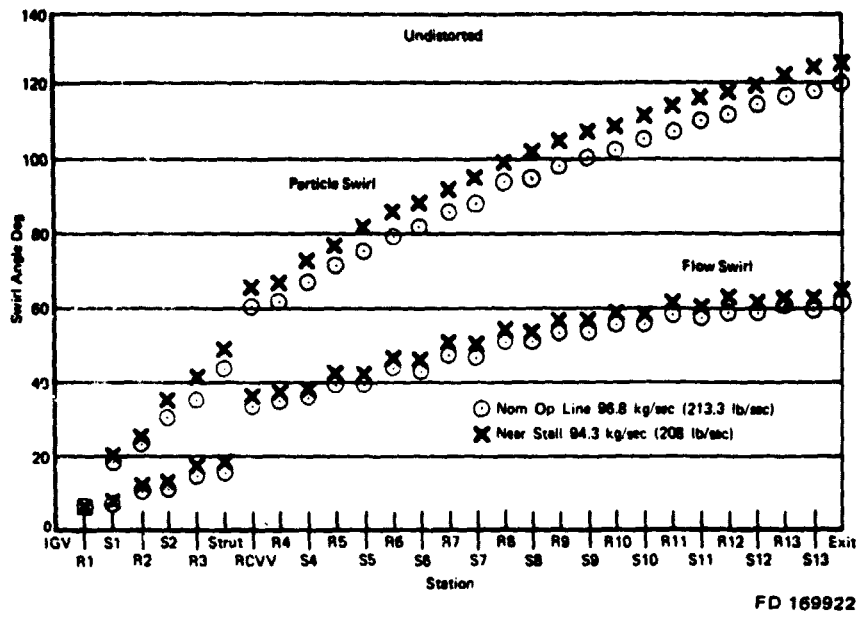

Figure 23. Swirl Through Core Engine - Individual Distortion

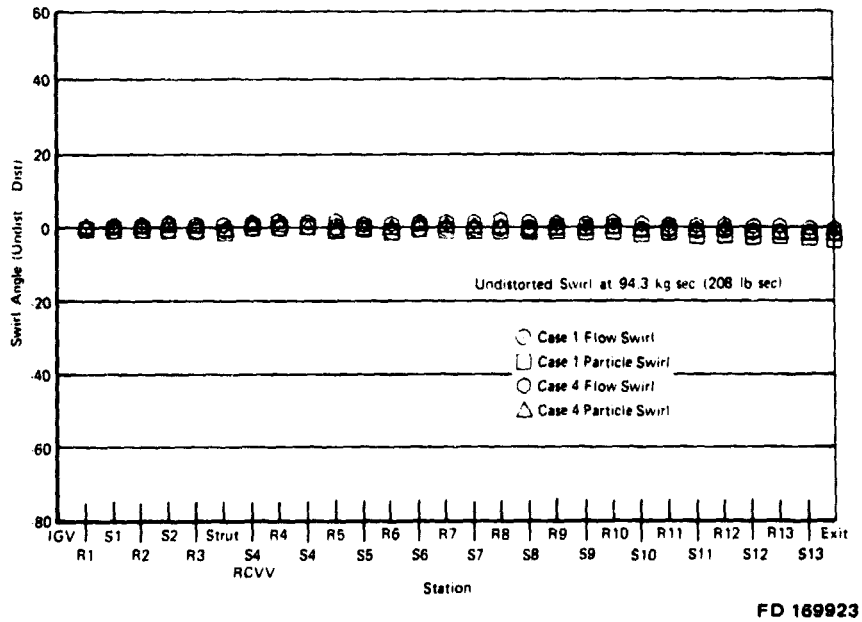

Figure 24. Variation in Swirl Due to Distortion

*Table 2. Relative Swirl Angles: Flow Swirl Undistorted — Flow Swirl Distorted**

Case Station	1	2	3	4	5	6	7
1	0.0	0.0	0.0	0.0	0.0	0.0	0.0
2	−0.1	−0.1	0.0	1.2	0.9	1.2	−0.8
3	−0.1	0.1	−0.2	0.8	0.7	1.1	−0.8
4	−0.1	0.0	−0.3	0.7	0.7	1.1	−0.9
5	0.1	0.4	−0.3	0.8	0.7	1.1	−0.7
6	0.0	0.3	−0.3	0.8	0.6	1.1	−0.8
7	3.7	5.3	−0.3	3.2	−1.2	0.9	−1.6
8	3.7	5.3	−0.3	3.2	−1.2	0.9	−1.6
9	0.0	0.0	0.0	0.0	0.0	0.0	0.0
10	−0.1	−0.1	0.0	1.6	1.3	1.6	−1.1
11	−0.1	0.0	−0.1	1.4	1.1	1.5	−1.2
12	0.0	0.1	−0.0	1.5	0.4	1.5	−1.1
13	−0.1	0.2	−0.1	1.3	1.0	1.3	−1.2
14	−0.1	0.2	−0.1	1.3	1.1	1.3	−1.1
15	−0.4	−0.2	−0.3	0.9	1.5	1.3	−0.7
16	0.6	0.7	0.6	1.9	2.5	2.2	0.3
17	0.6	0.9	0.6	2.1	2.8	2.2	0.5
18	0.5	0.9	0.6	2.0	2.8	2.6	0.5
19	0.6	1.2	0.6	2.3	3.1	2.9	0.7
20	0.5	1.1	1.1	2.2	3.0	2.8	0.6
21	0.5	1.3	1.3	2.4	3.4	3.3	0.7
22	0.4	2.3	2.3	2.3	3.3	3.3	0.7
23	0.5	1.3	1.3	2.4	3.3	3.3	0.7
24	0.3	1.1	1.1	2.2	3.2	3.3	0.5
25	0.3	1.2	1.2	2.3	3.2	3.3	0.5
26	0.2	1.0	1.0	2.2	3.0	3.3	0.3
27	0.2	1.0	0.3	2.1	3.0	3.2	0.3
28	0.0	0.8	0.2	2.0	2.8	3.1	0.0
29	0.1	0.9	0.2	2.0	2.8	3.1	0.1
30	−0.2	0.6	0.1	1.8	2.5	3.0	−0.3
31	−0.1	0.6	0.1	1.8	2.5	3.0	−0.2
32	−0.4	0.4	−0.1	1.6	2.2	2.8	−0.6
33	−0.3	0.4	−0.1	1.6	2.2	2.8	−0.6
34	−0.7	0.2	−0.2	1.4	1.8	2.6	−0.1
35	−0.6	0.1	−0.3	1.4	1.9	2.4	−1.0
36	−0.9	−0.2	−0.5	1.2	1.5	2.3	−1.5
37	−0.9	−0.2	−0.5	1.1	1.4	2.3	−1.5

Table 2. Relative Swirl Angles: Particle Swirl Undistorted — Particle Swirl Distorted (Continued)*

Case Station	1	2	3	4	5	6	7
1	0.0	0.0	0.0	0.0	0.0	0.0	0.0
2	−0.1	−0.1	0.0	1.2	0.9	1.2	−0.8
3	−0.2	0.1	−0.5	0.3	0.5	1.1	−0.8
4	−0.3	0.0	−0.6	0.2	0.5	1.0	−0.8
5	−0.1	0.5	−0.7	0.2	0.4	1.0	−0.7
6	−0.2	0.4	−0.7	0.2	0.4	1.1	−0.7
7	6.4	8.9	3.3	4.8	−1.3	1.7	−0.9
8	5.4	7.9	2.3	3.8	−2.3	0.7	−1.9
9	0.0	0.0	0.0	0.0	0.0	0.0	0.0
10	0.1	−0.1	0.0	1.6	1.3	1.6	−1.1
11	−0.4	−0.1	−0.3	0.8	1.0	1.1	−1.2
12	−0.4	−0.1	−0.3	0.9	1.1	1.2	−1.1
13	−0.5	0.2	−0.4	0.5	0.9	0.7	−1.1
14	−0.4	0.3	−0.3	0.6	1.0	0.8	−0.9
15	−1.07	−0.42	−0.81	−0.2	1.42	0.61	−0.53
16	0.0	0.58	0.19	0.86	2.52	1.61	0.57
17	0.0	0.81	0.21	1.1	2.81	1.93	0.75
18	−0.1	0.75	0.11	0.9	2.91	2.27	0.81
19	−0.8	1.03	0.12	1.1	3.25	2.64	1.01
20	−0.3	0.84	−0.06	0.9	3.16	2.77	0.86
21	−0.2	1.11	−0.03	1.1	3.48	3.12	1.09
22	−0.5	0.89	−0.15	0.9	3.31	3.21	0.86
23	−0.6	0.81	−0.23	0.8	3.24	3.13	0.78
24	−0.81	0.57	−0.38	0.5	3.00	3.16	0.48
25	−0.8	0.58	−0.38	0.7	3.02	3.17	0.5
26	−1.1	0.23	−0.64	0.3	2.62	3.01	0.03
27	−1.1	0.26	−0.61	0.4	2.65	3.05	0.06
28	−1.5	−0.15	−0.9	0.0	2.15	2.83	−0.52
29	−1.4	−0.1	−0.85	0.0	2.2	2.87	−0.47
30	−1.8	−0.53	−1.12	−0.3	1.67	2.62	−1.1
31	−.9	−0.6	−1.2	−0.4	1.59	2.55	−1.17
32	−2.4	−1.15	−1.57	−0.9	0.9	2.16	−1.97
33	−2.3	−1.12	−1.53	−0.8	0.93	2.19	−1.94
34	−2.9	−1.7	−1.92	−1.3	0.19	1.76	−2.79
35	−2.9	−1.73	−1.95	−1.3	0.16	1.73	−2.82
36	−3.5	−2.44	−2.43	−1.9	−0.76	1.16	−3.87
37	−3.45	−2.38	−2.37	−1.9	−0.7	1.22	−3.81

*Near-Stall Point

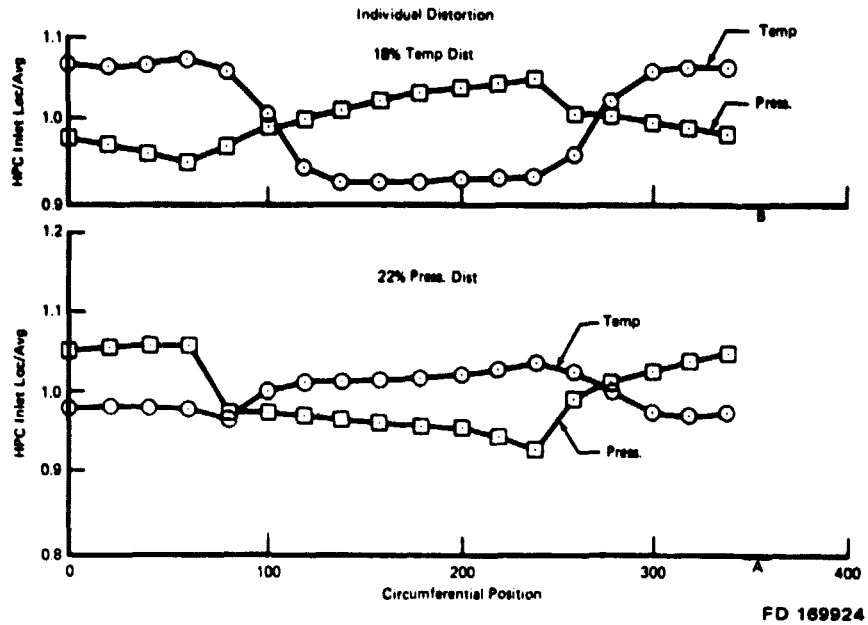

Figure 25. Fan Exit Distortion Comparison

The F100(3) fan characteristics, incorporated into the distortion model, were defined using an adjusted wheel speed. This wheel speed varies with bypass ratio and is related to the fan flow (PHI) and pressure rise characteristics, as shown in figure 37. As part of the individual distortion analysis, an attempt was made to determine the distorted bypass ratio of the engine. This required manually iterating input bypass ratio to maintain the high compressor operating point on its operating line while backpressuring the fan bypass stream until fan stall occurred. Because of the difficulty and time required to complete such an iteration, an evaluation of the impact of bypass ratio (BPR) on response predictions was made to determine if a constant value of BPR could be used for distortion analysis.

Figure 38 shows the effect of small bypass ratio variations on the predicted fan stall line and distortion sensitivity with the case 3 (15% $\Delta P/P$) distortion pattern. Although bypass ratio did affect the flow at which stall was predicted to occur, the variation in distortion sensitivity with flow closely followed the empirical data. Therefore, reasonable predictions resulted at a fixed bypass ratio that corresponded to operation on the nominal fan operating line. In addition, variations had only a small effect on the fan distortion transfer characteristics, as shown in figure 39. However, variations in bypass ratio significantly affected the high pressure compressor operating point as can be seen in figure 40.

As noted in the Approach Section of this report, the fan stall point was determined by increasing the fan exit static pressure until stall is predicted. This required specifying the incremental step in exit static pressure the model uses in searching for a stall point (see Appendix II). Variations in this step size were found to affect the predicted stall point as shown in figure 41. While the distorted speed line is insensitive to the step size, figure 42 shows that the predicted stall point varied due to the flatness of the speed line near the stall point. As a result, the smallest step size of 1.001 is recommended for accurately defining stall points.

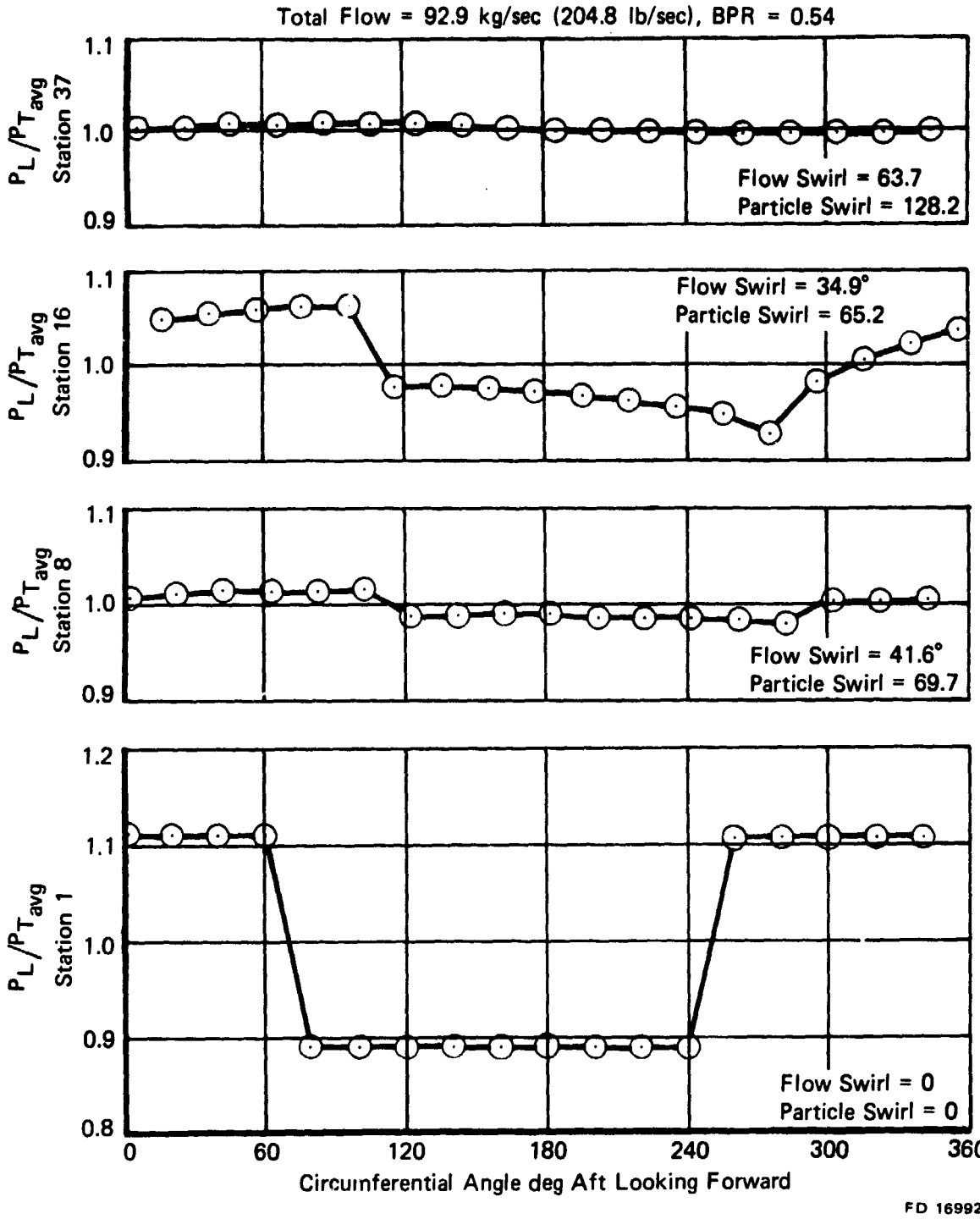

Figure 26. Pressure Profile at Engine Major Stations Due to (22% ΔP/P/180 deg) Inlet Distortion

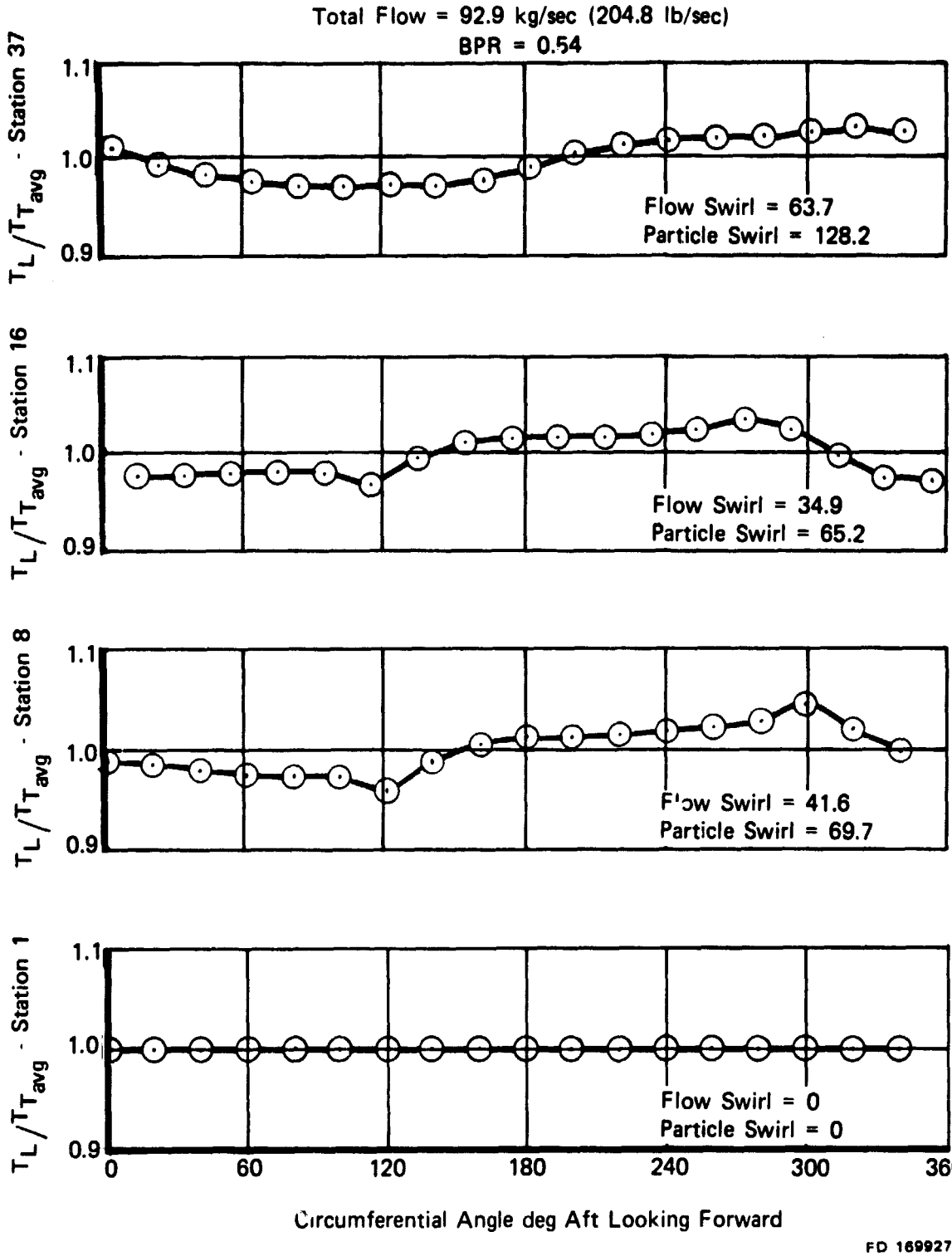

Figure 27. Temperature Profile at Engine Major Stations Due to (22[illegible] ΔP/P/ 180 deg) Inlet Distortion

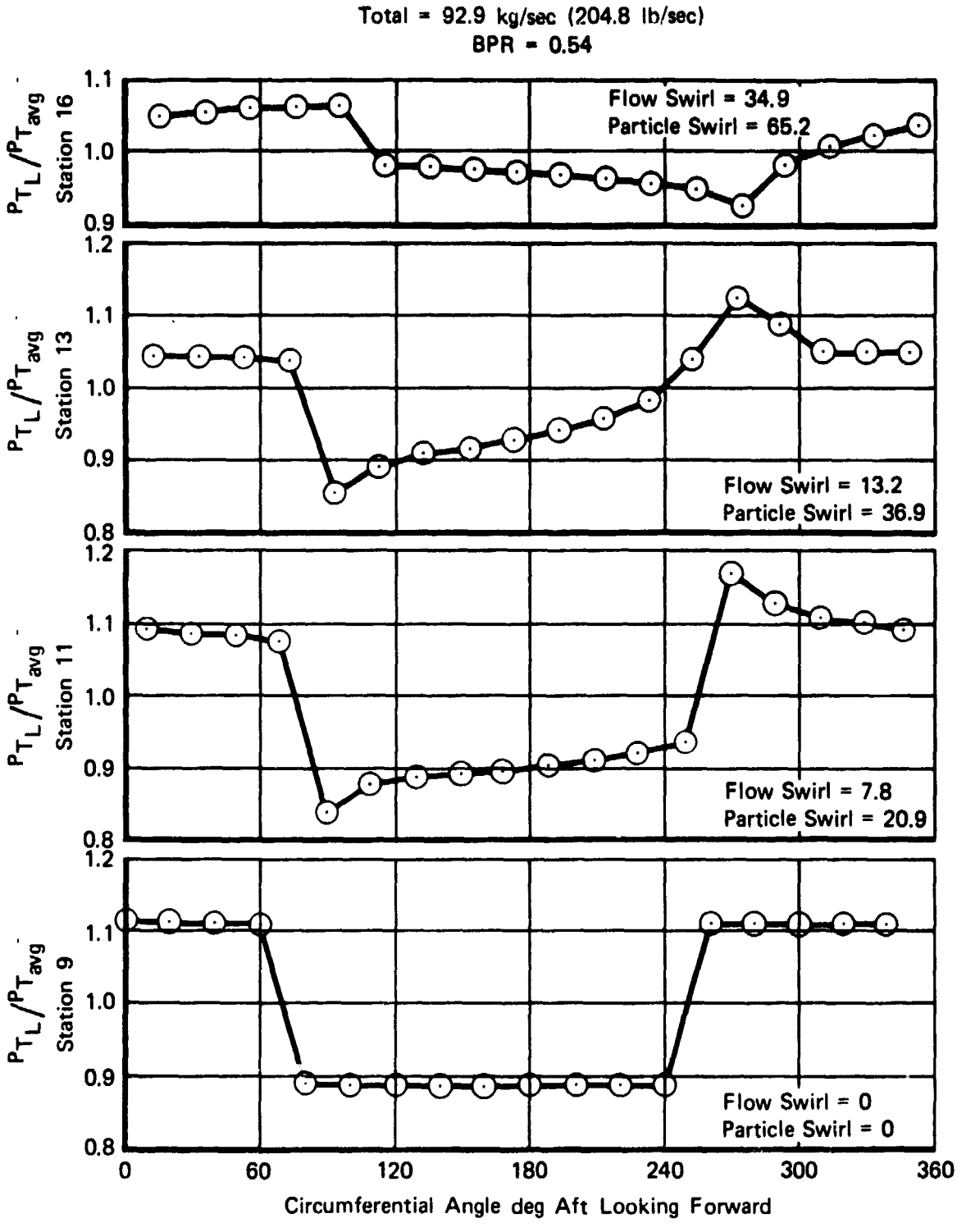

Figure 28. Pressure Profile Through the Fan Core Section Due to (22°; ΔP/P/180 deg) Inlet Distortion

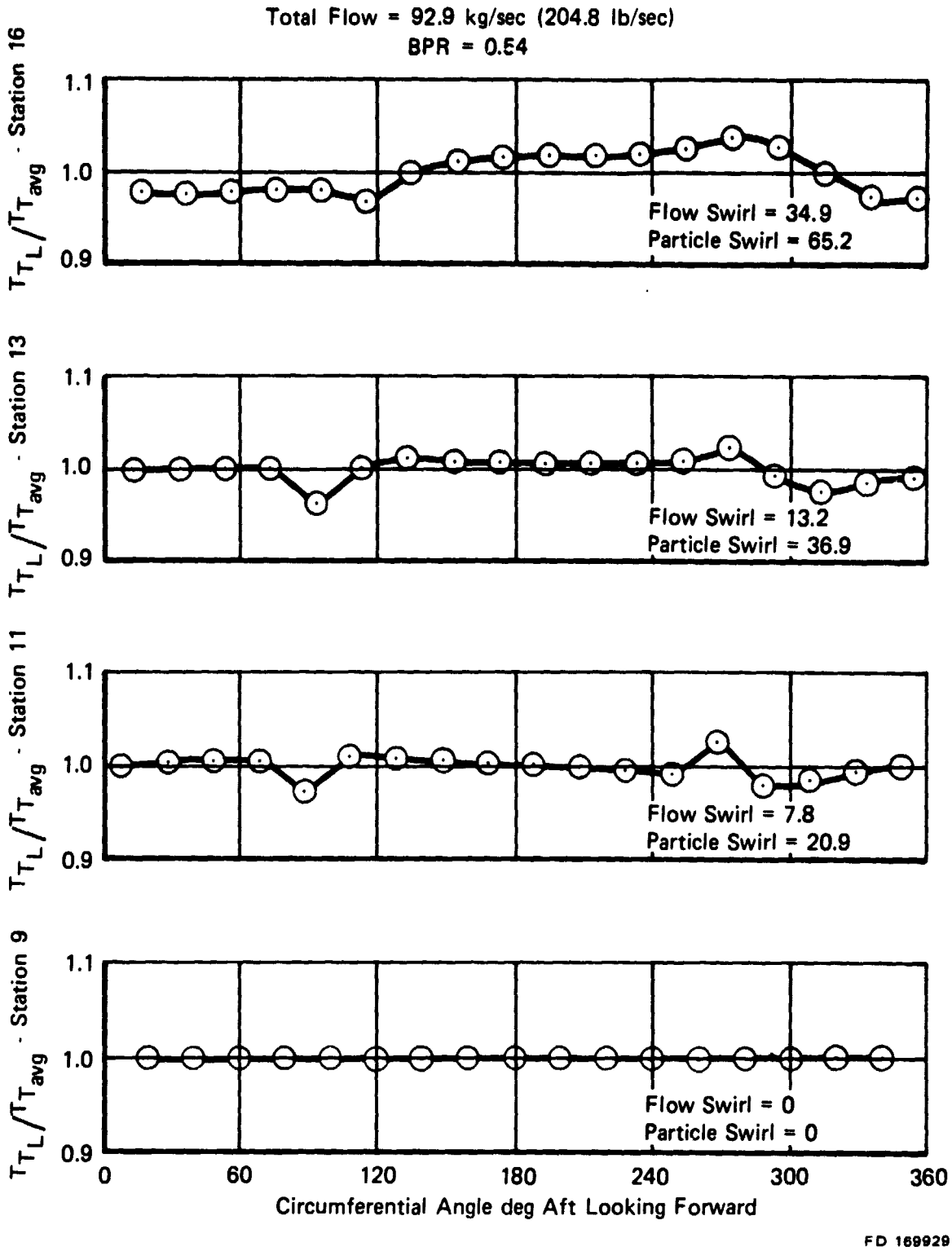

Figure 29. Temperature Profile Through the Fan Core Section Due to (22° ΔP/P/180 deg) Inlet Distortion

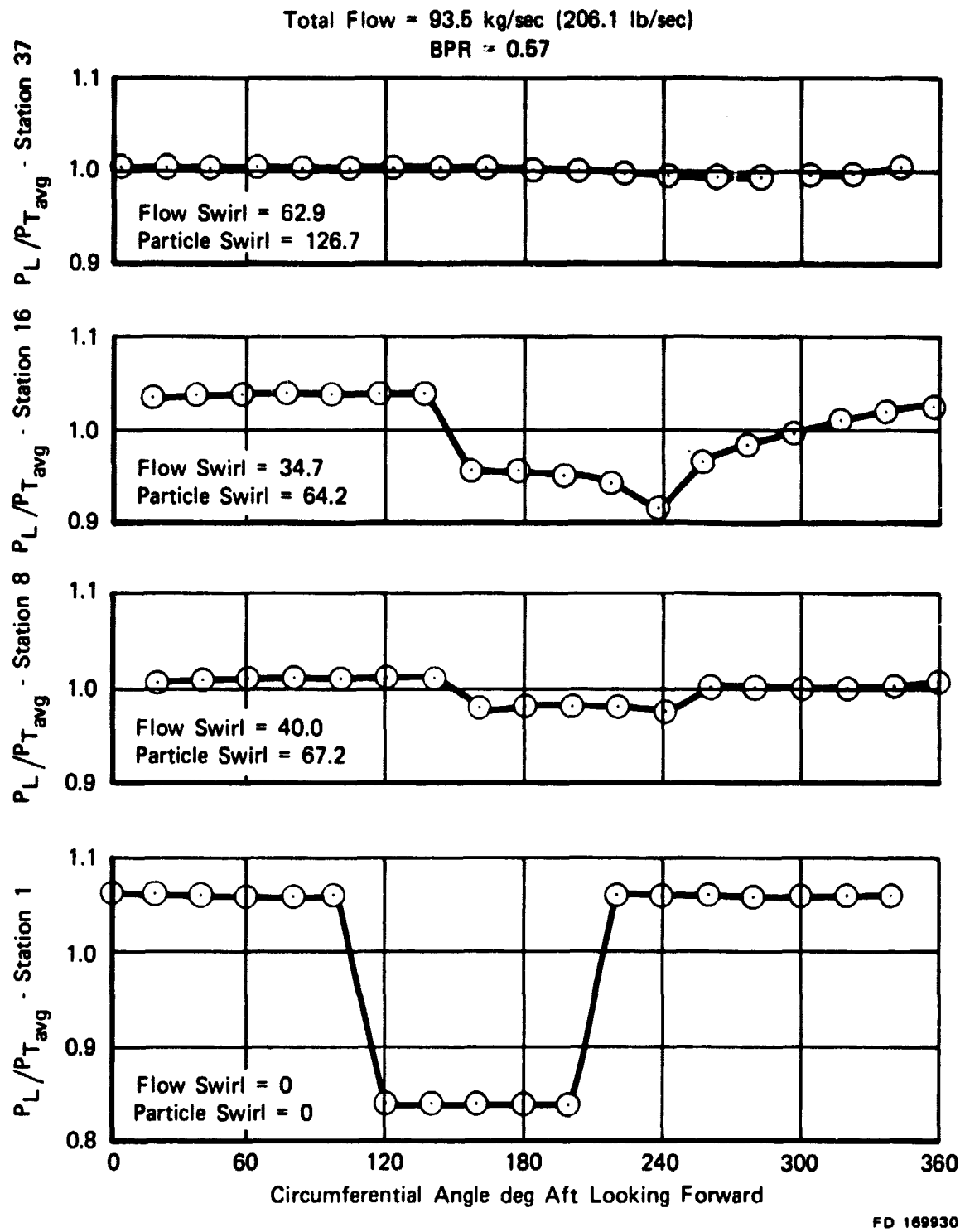

Figure 30. Pressure Profile at Engine Major Stations Due to (22° ΔP/P/90 deg) Inlet Distortion

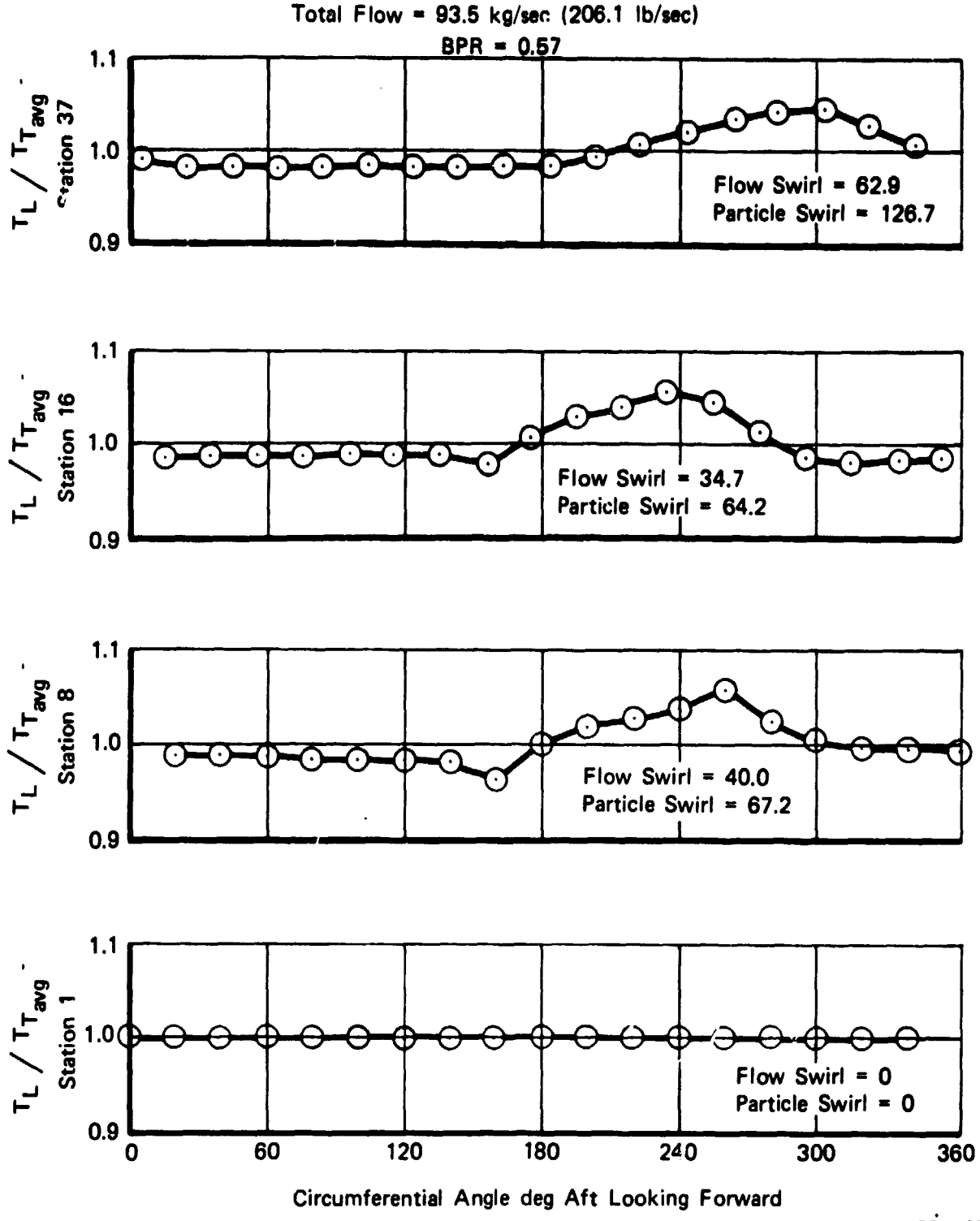

Figure 31. Temperature Profile at Engine Major Stations Due to (22°C ΔP/P/ 90 deg) Inlet Distortion

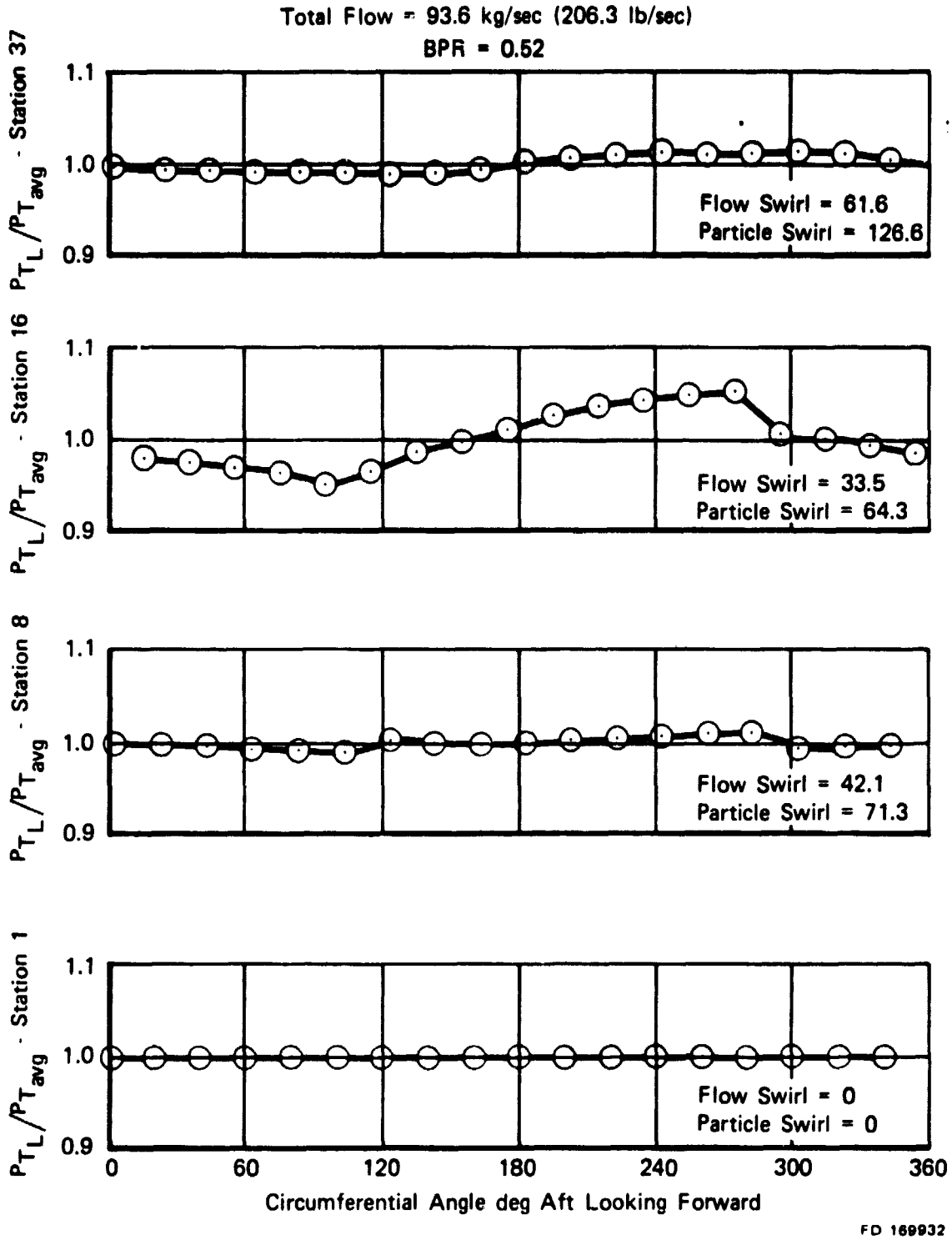

Figure 32. Pressure Profile at Engine Major Stations Due to (180 $\Delta T/T$/180 deg) Inlet Distortion

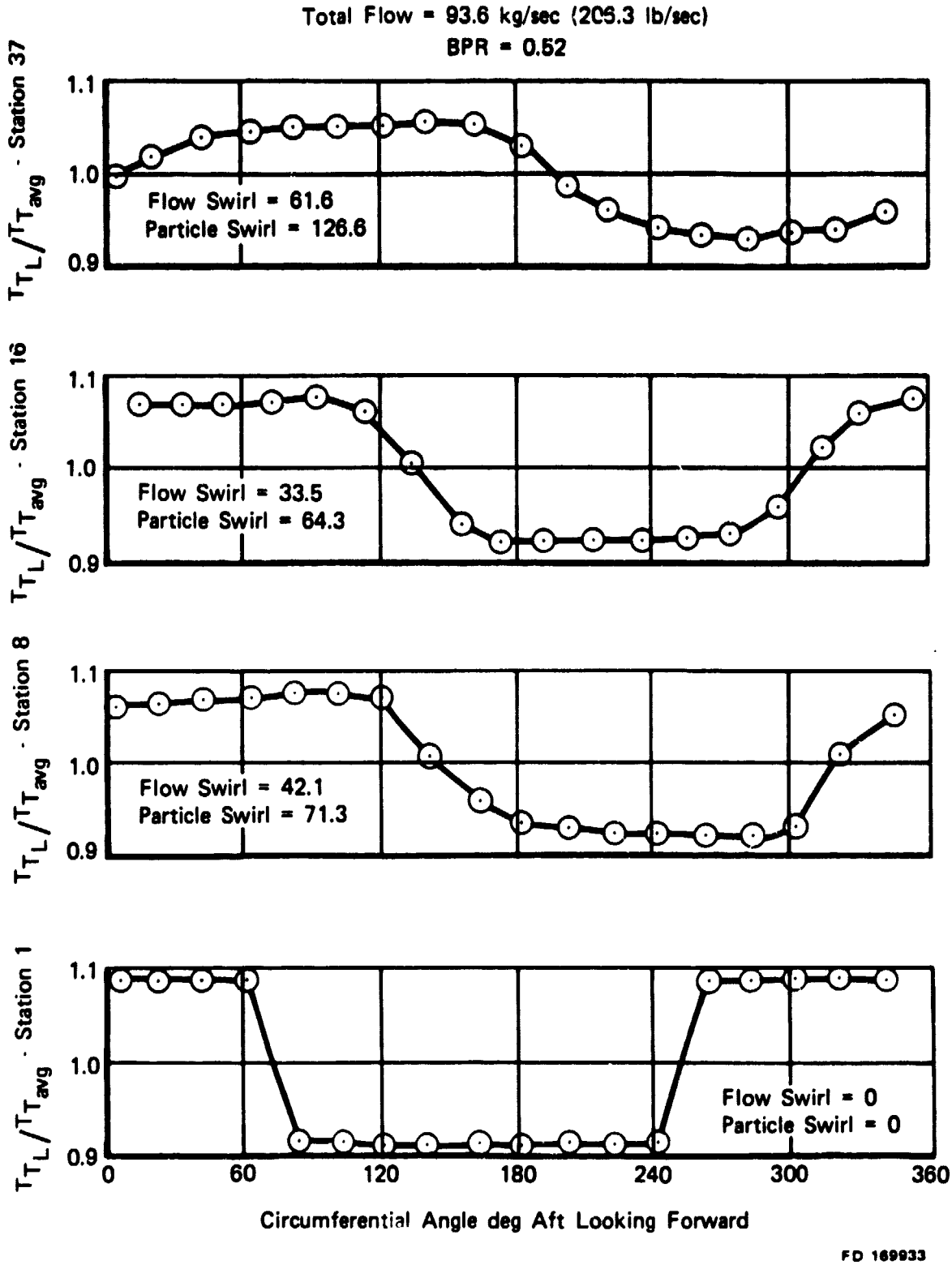

Figure 33. Temperature Profile at Engine Major Stations Due to (18° ΔT/T/180 deg) Inlet Distortion

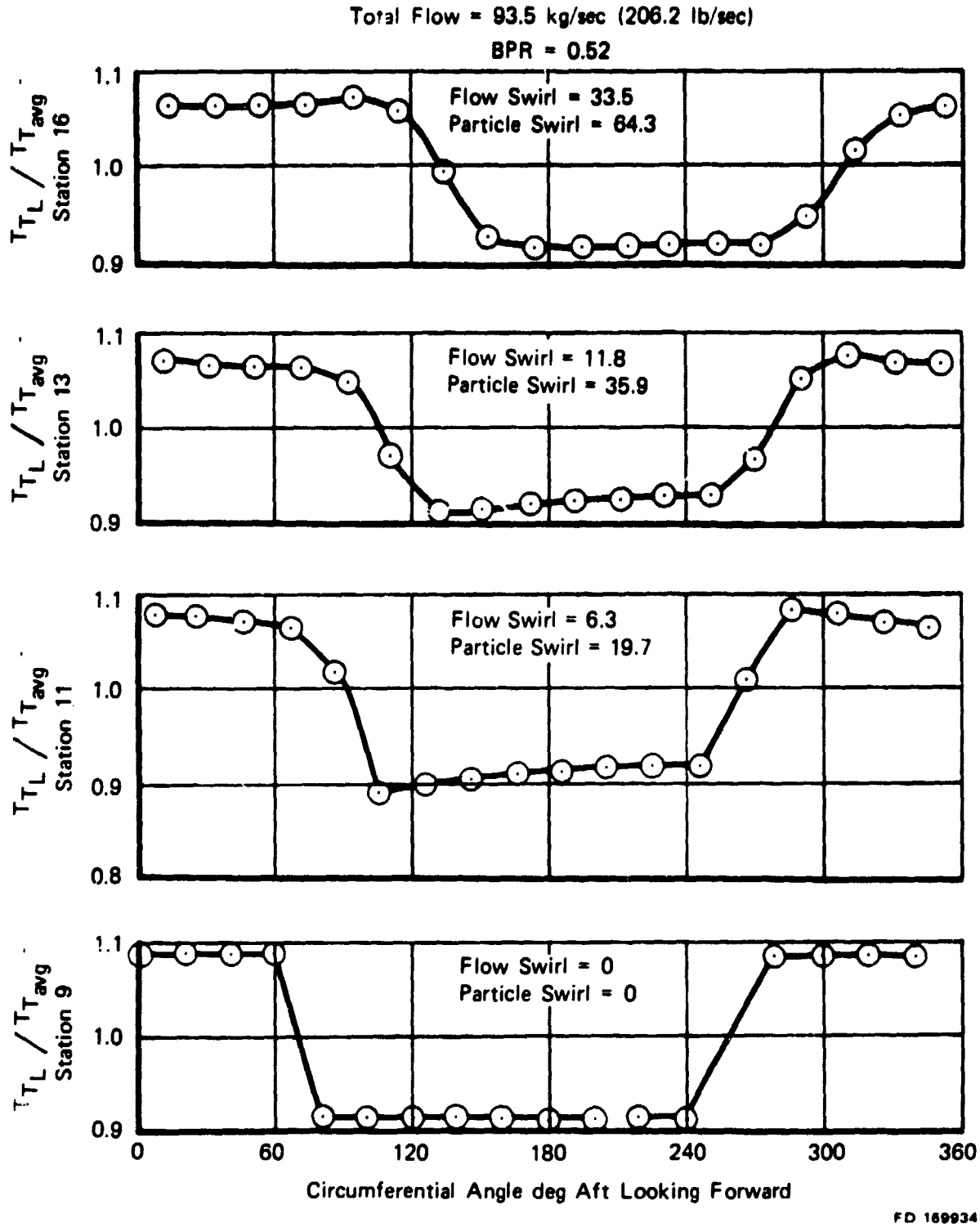

Figure 34. Temperature Profile Through the Fan Core Section Due to (18°, ΔT/T/180 deg) Inlet Distortion

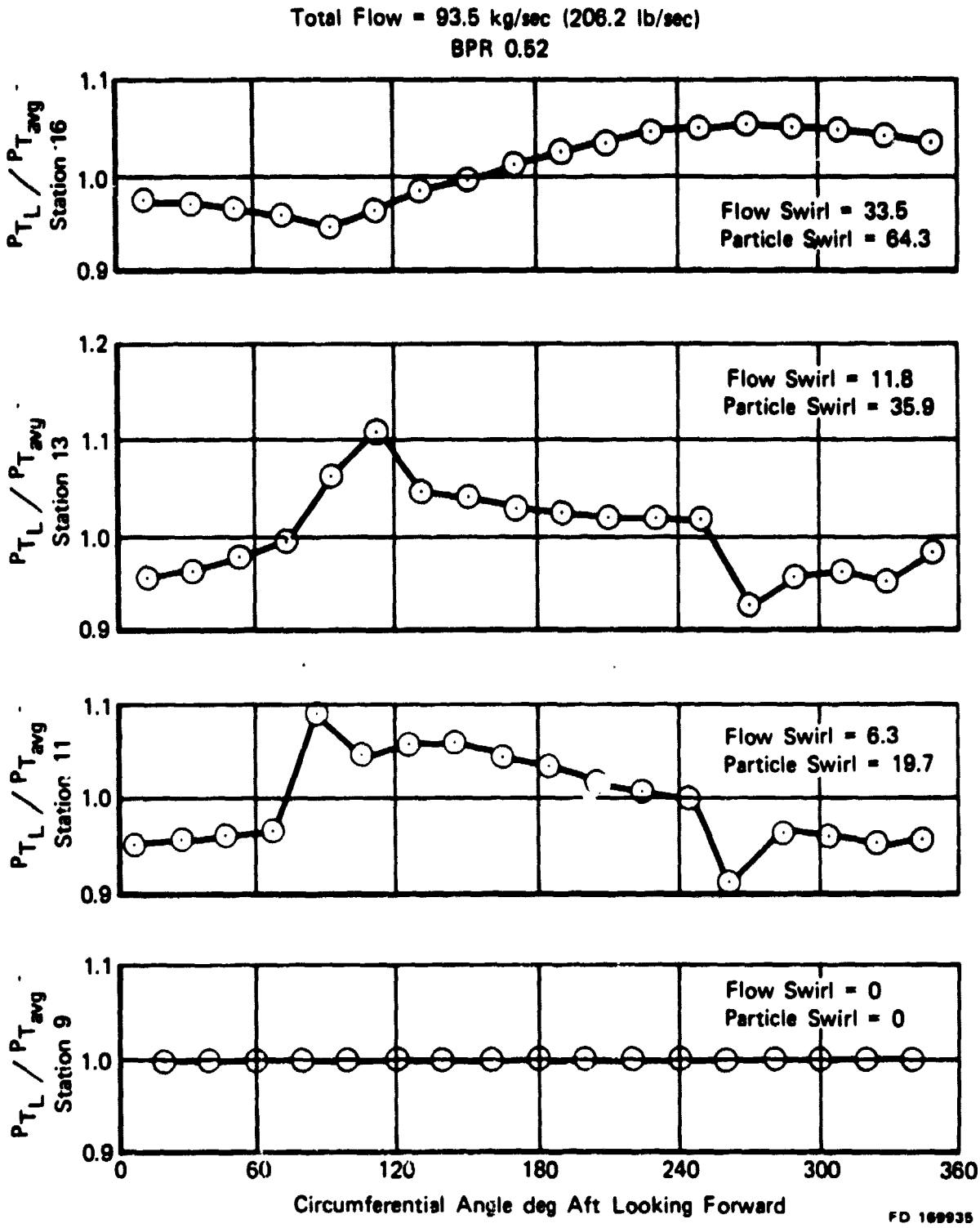

Figure 35. Pressure Profile Through the Fan Core Section Due to (18° ΔT/T/180 deg) Inlet Distortion

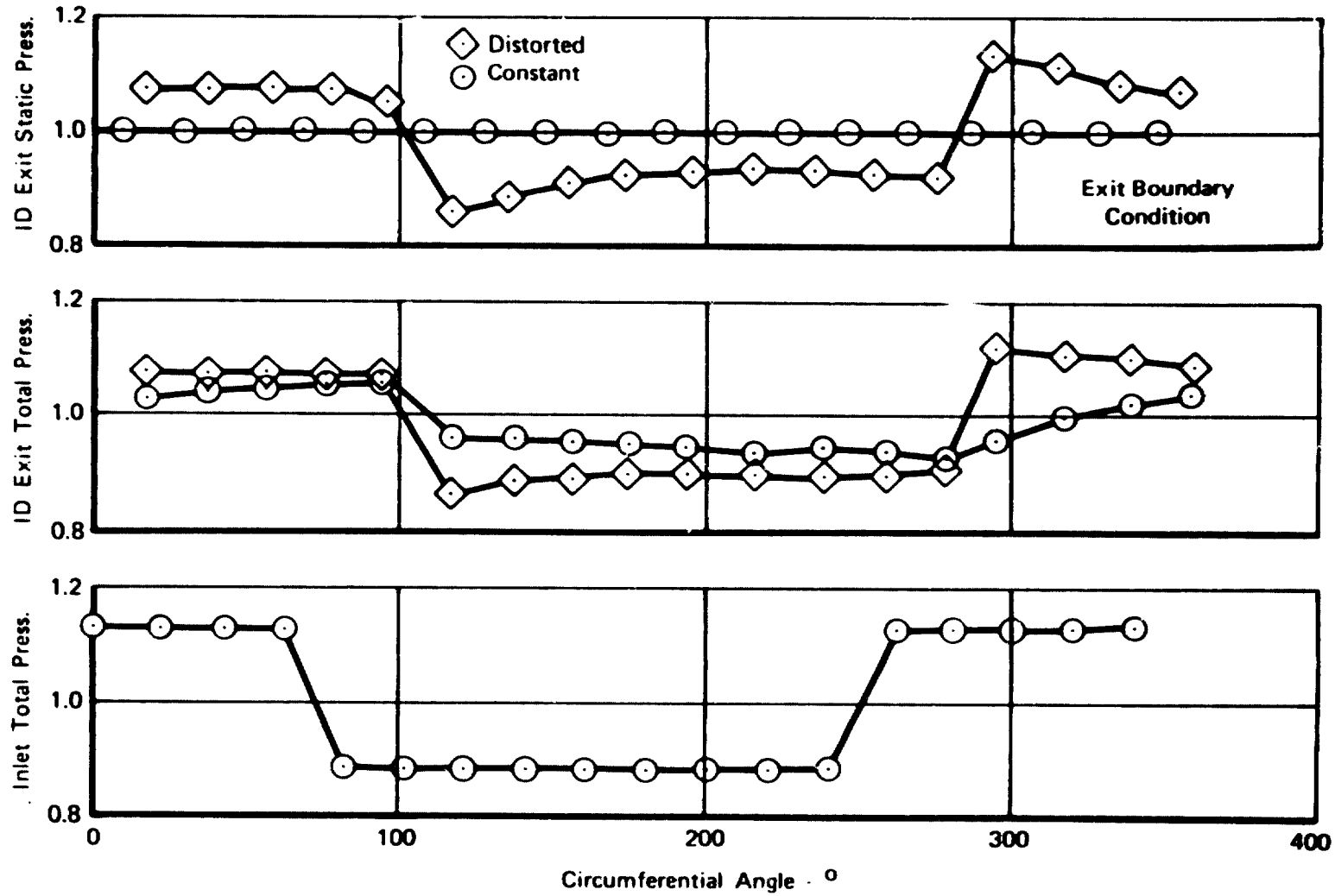

Figure 36. Exit Boundary Condition Effects: Response to Distortion

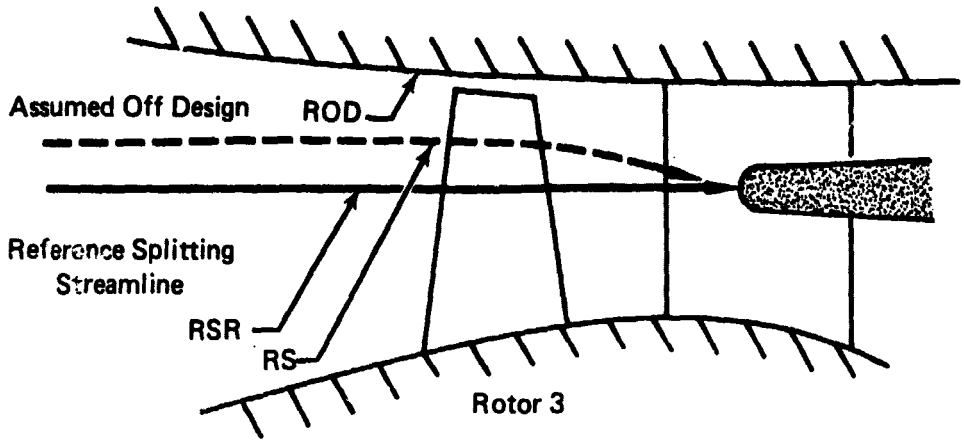

$$\frac{1}{\text{Wheel Speed}} = \frac{XND}{XNC(IRS)} \bullet \sqrt{\frac{ROD^2 + RSR^2}{ROD^2 + RS^2}} \rightarrow \frac{\text{U Reference BPR}}{\text{U Off Design BPR}}$$

$$PHI(IRS,J) = WAC(IRS,J) \bullet \frac{1}{\text{Wheel Speed}} \text{ / Area (IRS)}$$

$$PS(I+1,J) = [PSI(IRS,J) \bullet (\text{Wheel Speed})^2 + 1.] \bullet PS(I,J)$$

FD 169920

Figure 37. Bypass Ratio Effect on Fan Characteristics

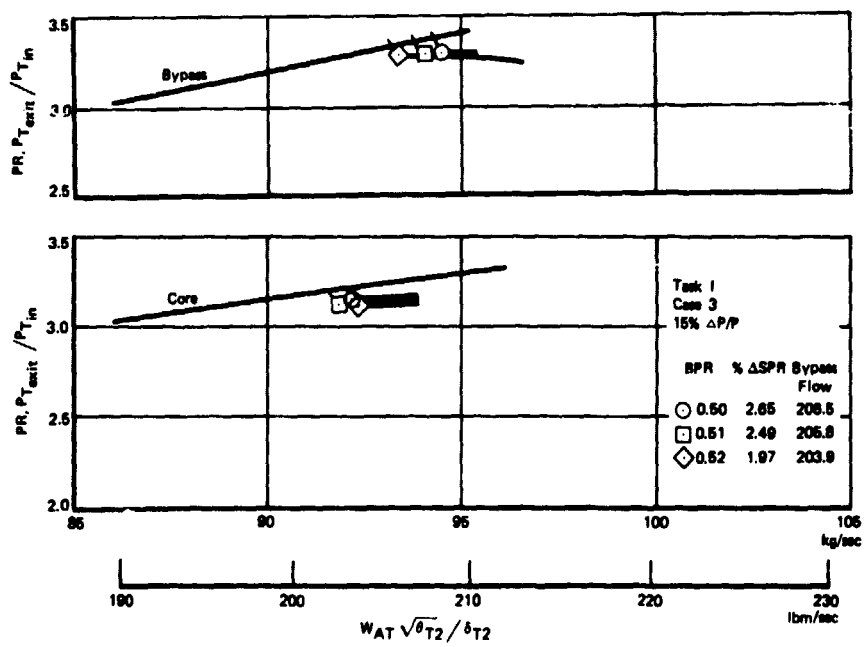

Figure 38. Effect of Bypass Ratio on Sensitivity

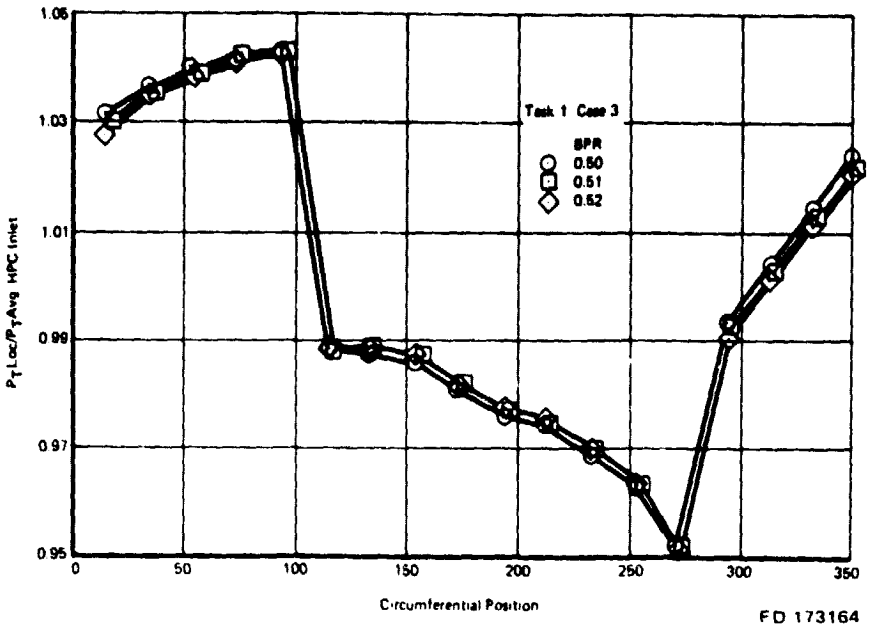

Figure 39. Effect of Bypass Ratio on Distortion Transfer Fan Core

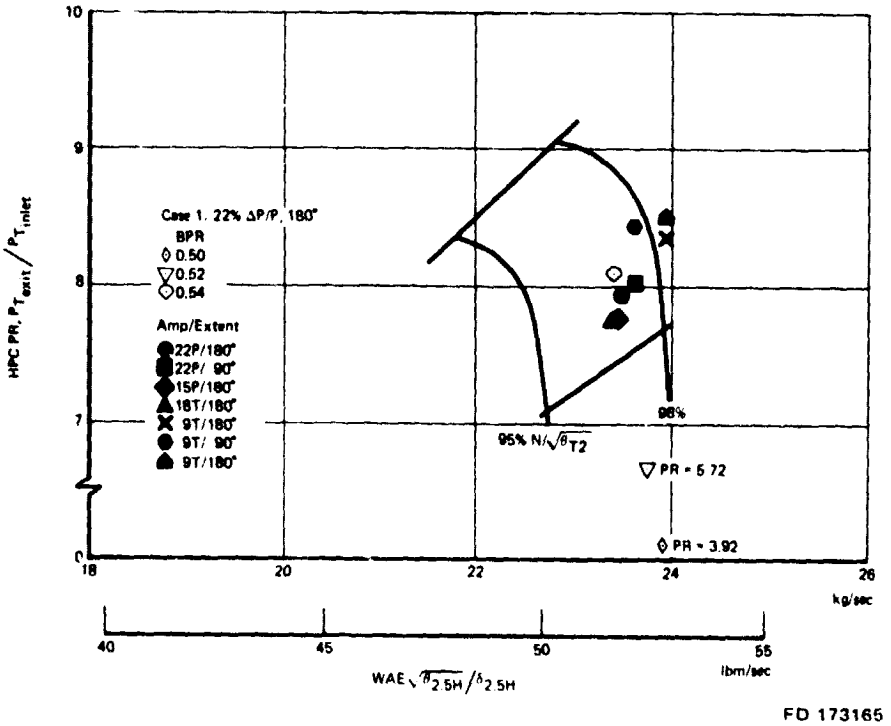

Figure 40. Task 1 HPC Match

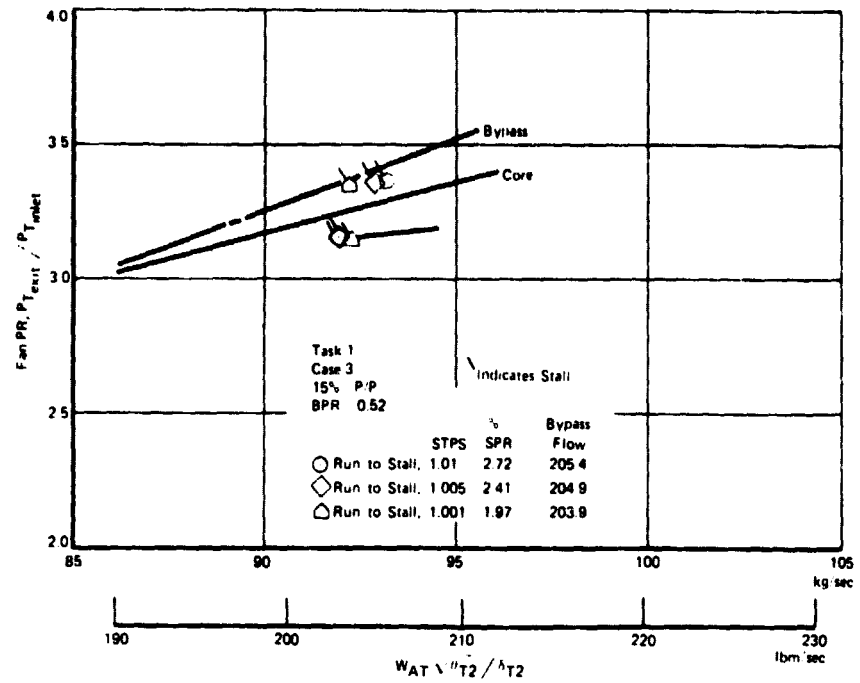

Figure 41. Effect of STPS on Stall Prediction

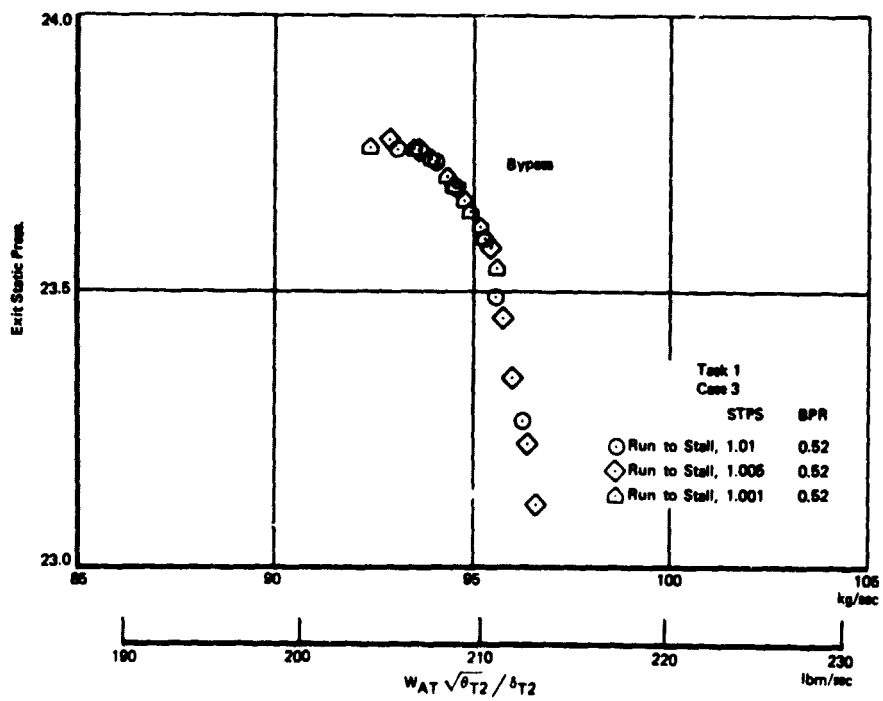

Figure 42. Effect of STPS on Static Pressure Rise

The multiple segment model also requires specifying the number of circumferential segments to be used in predicting distortion response. The larger the number of segments used, the more computation time is required for a given solution and the more accurate the prediction. Figure 43 shows a comparison of predicted fan stall points using 6 vs 18 circumferential segments. As can be seen, there is a significant difference in the two predictions. No attempt was made to optimize the number of segments for this study. Instead, eighteen segments were used for all cases to ensure reasonable accuracy.

COMBINED DISTORTION — SYSTEM ANALYSIS

Previous analysis of engine operation with combined pressure and temperature distortion has shown that the engine response characteristics depend on the relative orientations of the distortions, as well as the amplitudes and circumferential extents of the distortions (References 3 and 4). The five combined distortions used in this study were chosen to establish orientation effects.

Fan operation with combined distortion can result in both a high local pressure ratio due to the pressure distortion and a local variation in corrected speed due to the temperature distortion. Figure 44 shows schematically the effect of the orientation of the distortions on the local fan operating points. Points A and B show the fan operating points when only pressure distortion is present. The addition of aligned temperature distortion (low pressure area coincides with high temperature area) results in Point A operating at a lower corrected speed (Point C). Since Point C is closer to the fan surge line than Point A, the aligned distortion surge line should be lower than the pure pressure distortion surge line. Opposed temperature distortion results in Point B operating at a lower corrected speed (Point D). Therefore, the opposed distortion surge line should be higher than the pure pressure distortion surge line. Figure 45 presents the predicted fan surge lines for the combined distortion cases and. as expected, the distortion levels are significantly affected by the distortion orientation.

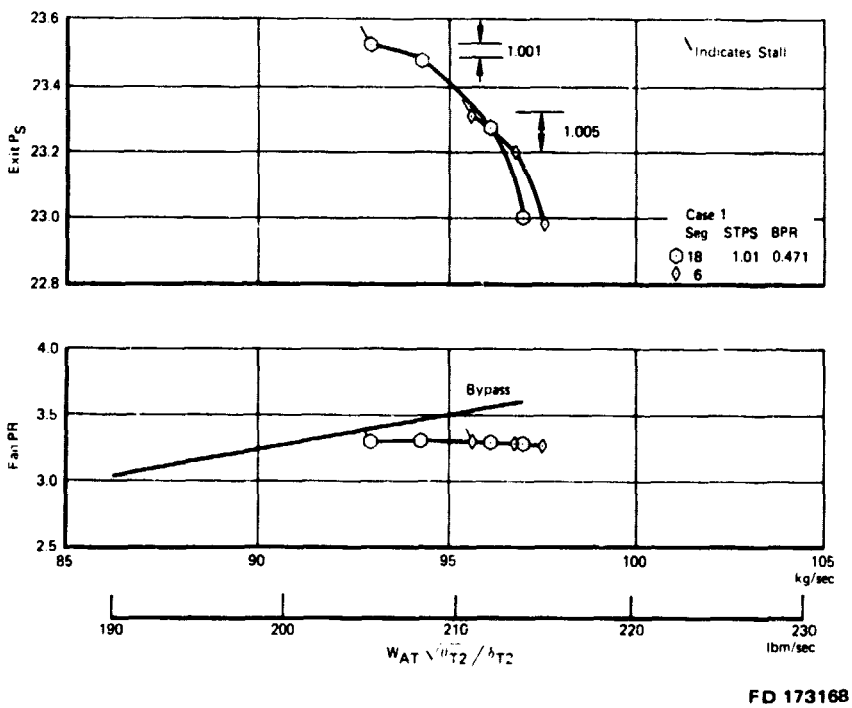

Figure 43. Effect of Segment Number on Stall Prediction

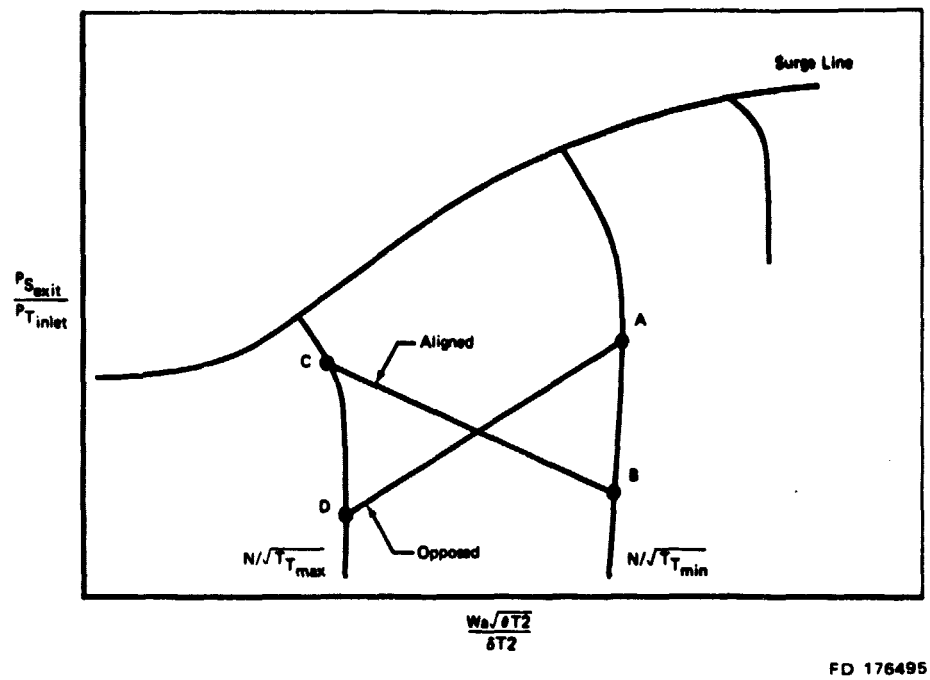

Figure 44. Effect of Combined Distortion on Fan Operation

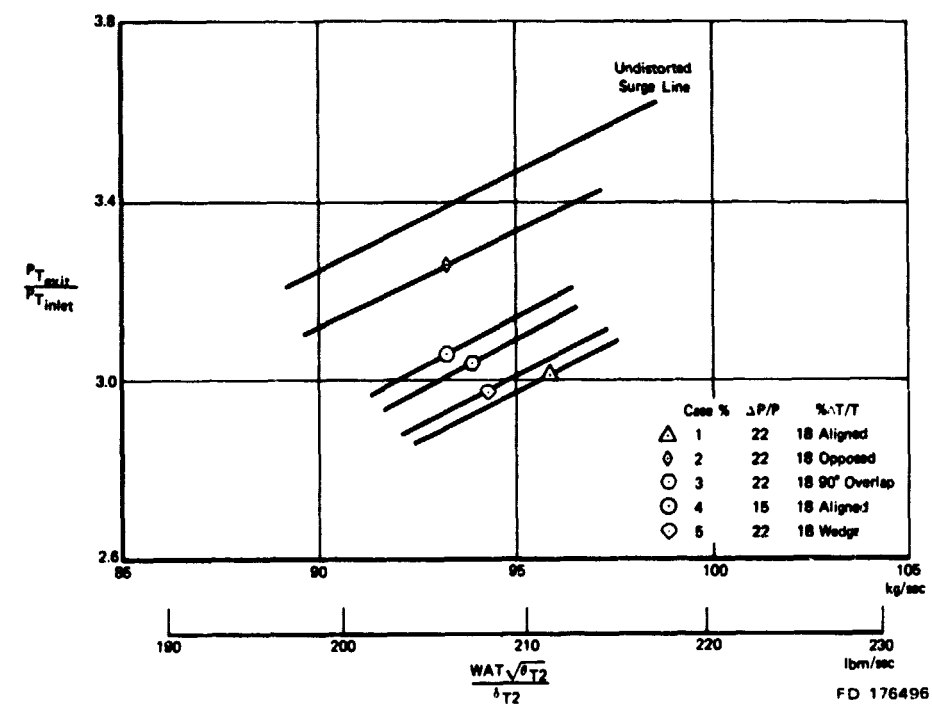

Figure 45. Predicted F100(3) Fan Surge Lines With Combined Distortion

An orientation correlation parameter was developed that relates the surge line level to the angular extent of the temperature distortion and angular overlap of the pressure and temperature distortions. The orientation parameter was designed to have a value of +1.0 for fully aligned distortions and −1.0 for opposed distortions. This is consistent with the resultant velocity distortions resulting from these distortion orientations. That is, fully aligned pressure and temperature distortion results in additive velocity distortions, while fully opposed distortions result in canceling velocity distortions. Figure 46 shows that surge line loss at a constant fan inlet airflow is a function of this orientation parameter. Also shown is the fan surge line level for the corresponding pure pressure distortion case. The aligned distortion results in a lower fan surge line than the pure pressure distortion, while the opposed distortion results in a higher surge line than the pure pressure distortion case. The other combined distortion surge lines fall between these extremes.

The level of fan exit pressure and temperature distortion were also found to depend on the relative orientation of the distortions at the fan inlet. Figures 47 through 50 show that predicted fan exit pressure and temperature distortion are a function of the combined distortion orientation parameter. The exit distortions for the aligned cases are predicted to be slightly higher than at the fan inlet. Fan exit distortions for the opposed case are predicted to be very low in level. Figure 51 shows that for the aligned case the generated temperature and pressure profiles add to the distortion transmitted by the fan while for the opposed case they reduce the exit distortion levels.

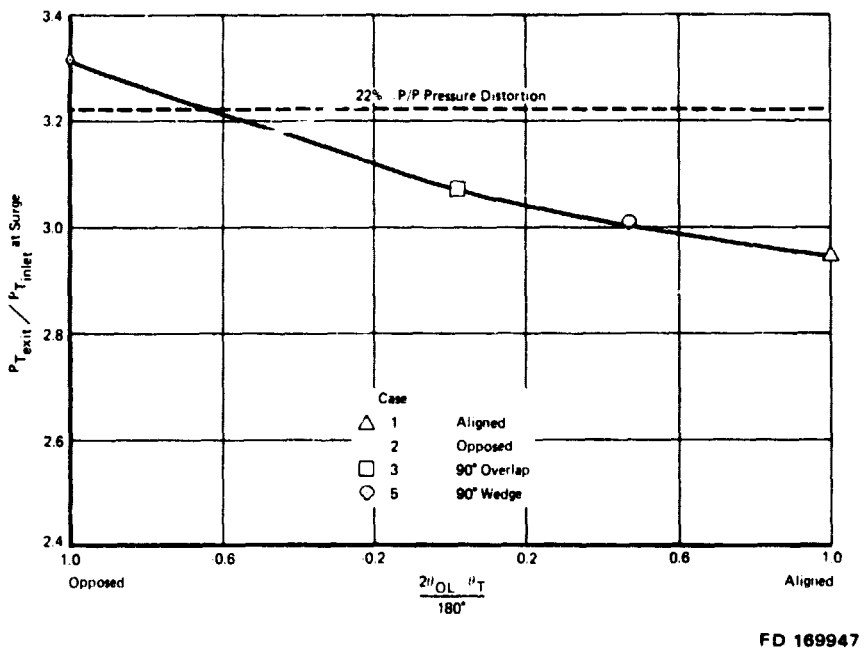

Figure 46. Fan Surge Line: Effect of Combined Distortion Orientation

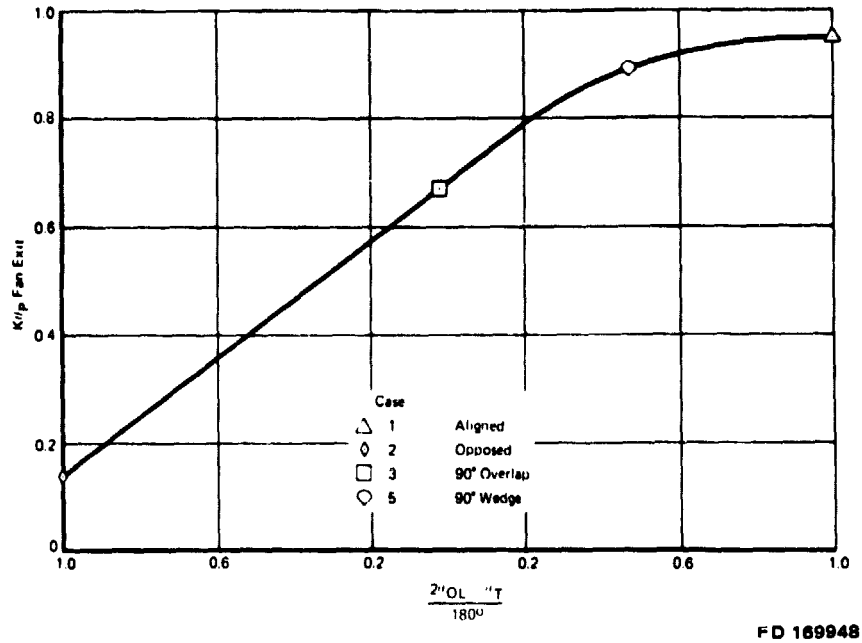

Figure 47. Predicted Fan Exit Distortion: Combined Distortion

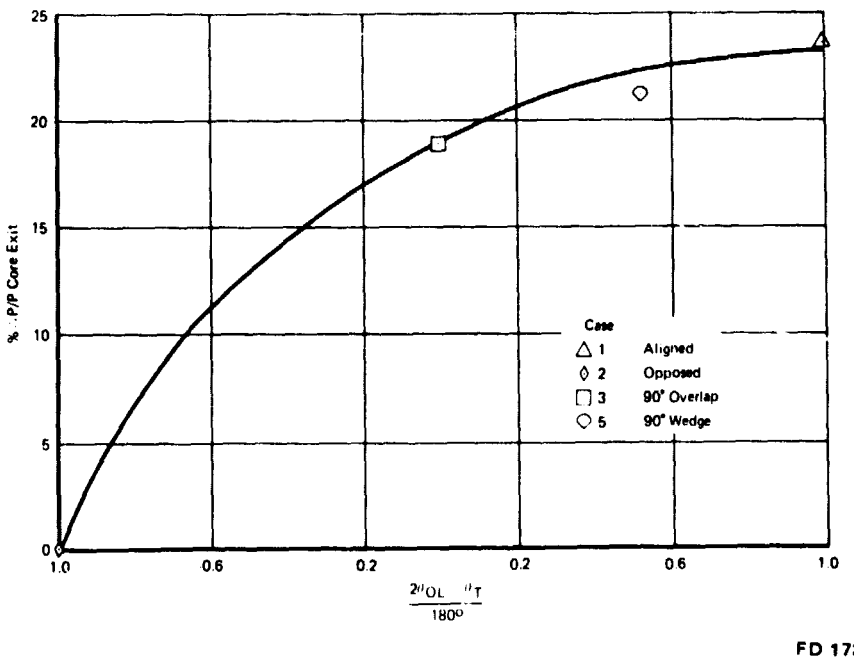

Figure 48. Predicted Fan Exit Combined Distortion (22% ΔP/P, 18% ΔT/T)

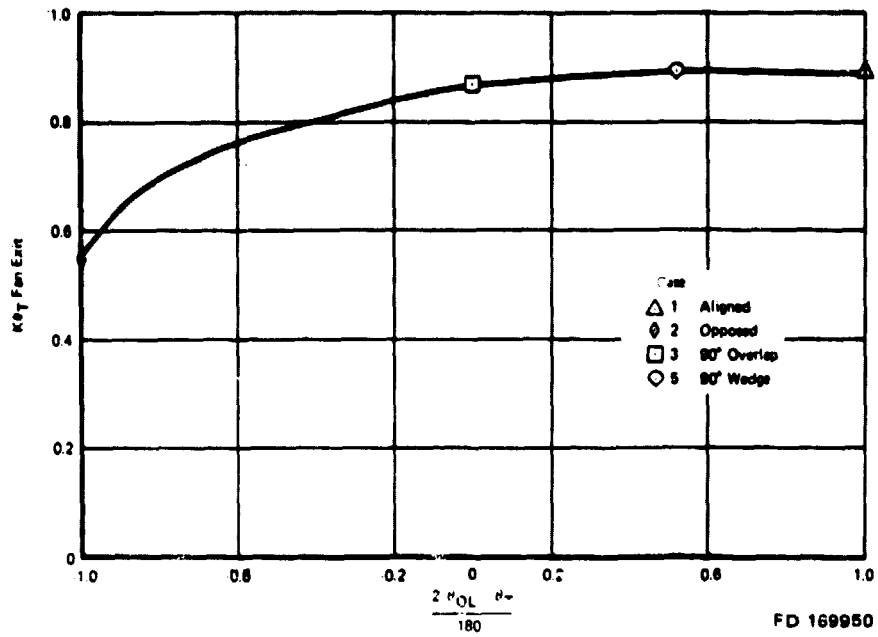

Figure 49. Predicted Fan Exit Combined Distortion: $K\theta_T$

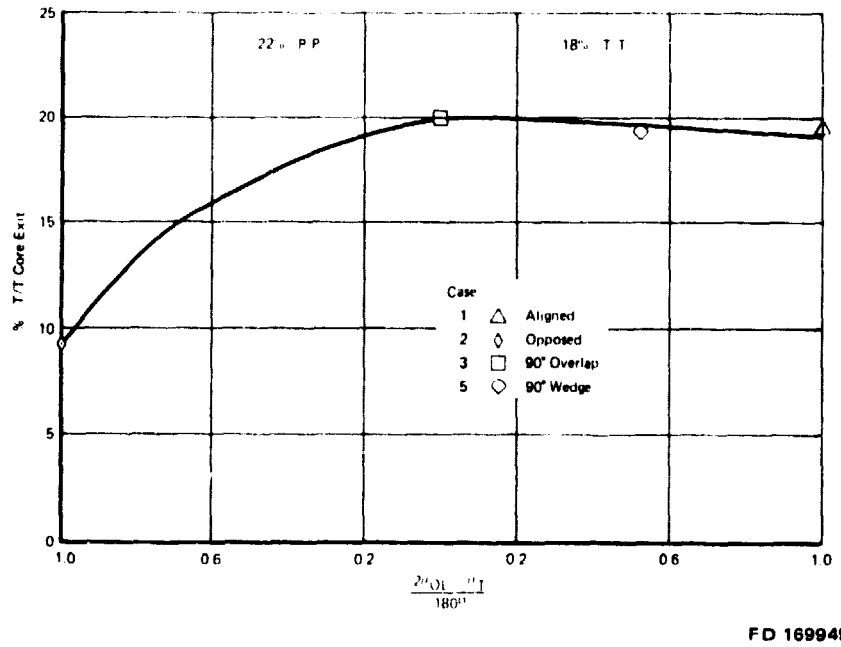

Figure 50. Predicted Fan Exit Combined Distortion: $\%\Delta T/T$ Core Exit

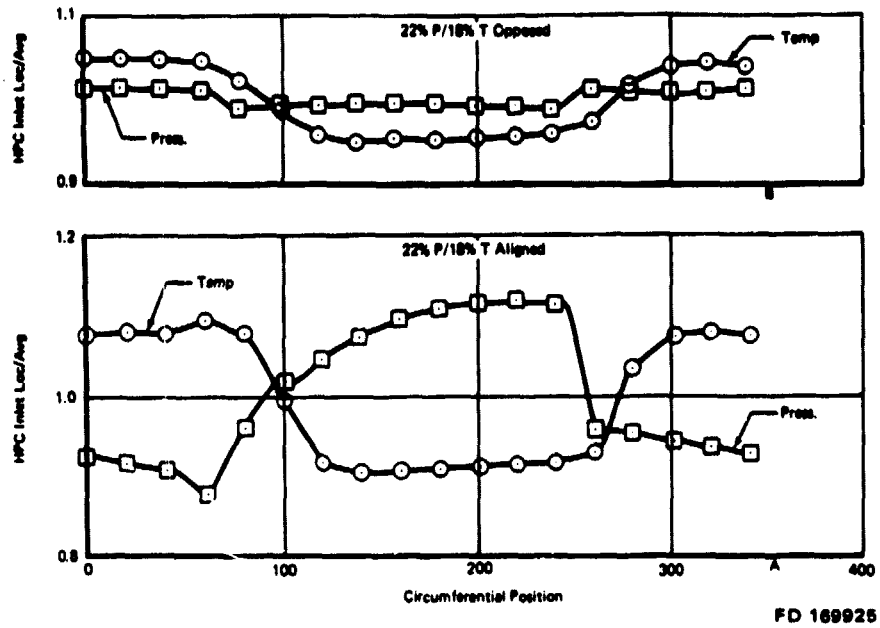

Figure 51. Fan Exit Combined Distortion Comparison

The feasibility of predicting fan response to combined distortion using individual distortion characteristics was also investigated. A distortion combination factor (DCF) was defined as a function of the overlap parameter which allows estimating the total surge line loss for a combined distortion by linearly combining the individual surge line losses (figure 52.). The following equation defines the use of DCF:

$$\%\Delta\ SPR_{ToT} = \%\ \Delta\ SPR_P + DCF\ (\%\ \Delta\ SPR_T)$$

where,

$\%\ \Delta\ SPR_{ToT}$ = Total loss in surge pressure
$\%\ \Delta\ SPR_P$ = Loss in surge pressure ratio due to pressure distortion
$\%\ \Delta\ SPR_T$ = Loss in surge pressure ratio due to temperature distortion.

This approach was found to give reasonable estimates as long as the pressure distortion was the predominant part of the combined distortion. Further development of the DCF approach is needed to account or combined cases where the temperature distortion predominates.

In addition, it was also found that the fan transfer characteristics for combined distortion could be estimated using individual distortion results. The method used in predicting the combined distortion transfer characteristics was to add the individual fan exit Kθp's when the inlet distortions were aligned or fully overlapped as in the 90 deg wedge case: subtract the exit K θp's and Kθt's when the inlet distortions were opposed. The 90 deg overlap case required additional analysis since it is neither aligned, fully overlapped or opposed. For this case it was assumed that one-third of the exit pressure distortion resulting from the inlet pressure distortion would be additive to the transmitted pressure distortion while one-third of exit temperature distortion resulting from the inlet pressure distortion would reduce the exit temperature distortion. These assumptions were based on the relative orientation of the exit distortions to the inlet distortions established in the individual distortion analysis.

Figure 53 shows the level of fan core exit pressure distortion based on combining individual distortion results vs the level predicted by the model for the combined distortion. As can be seen, excellent agreement exists between the combined individual results and actual predictions. Figure 54 shows a similar comparison for fan exit temperature distortion. Poorer agreement exists for the temperature distortion due to the wider variation in the phase relationship of the transmitted temperature distortion and generated temperature distortion. However, since most compressors are significantly less sensitive to temperature distortion than pressure distortion, more inaccuracy can be accepted in estimating the fan exit temperature distortion level.

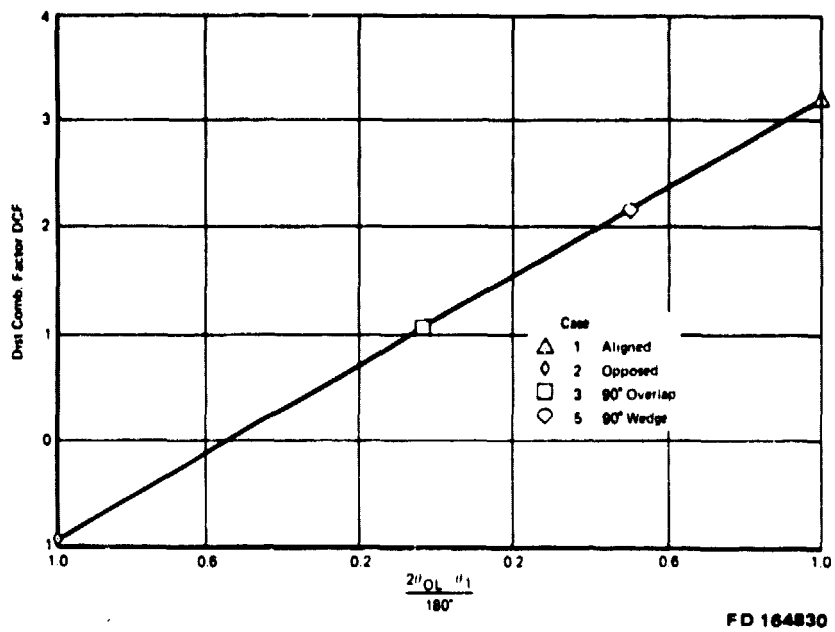

Figure 52. Combined Distortion Analysis

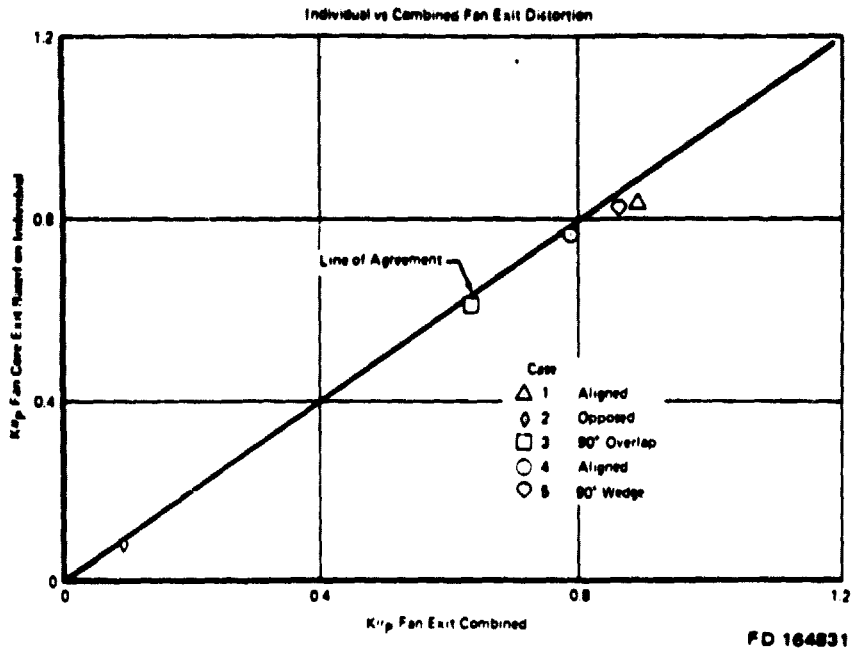

Figure 53. Combined Distortion Predictions: $K\theta_p$

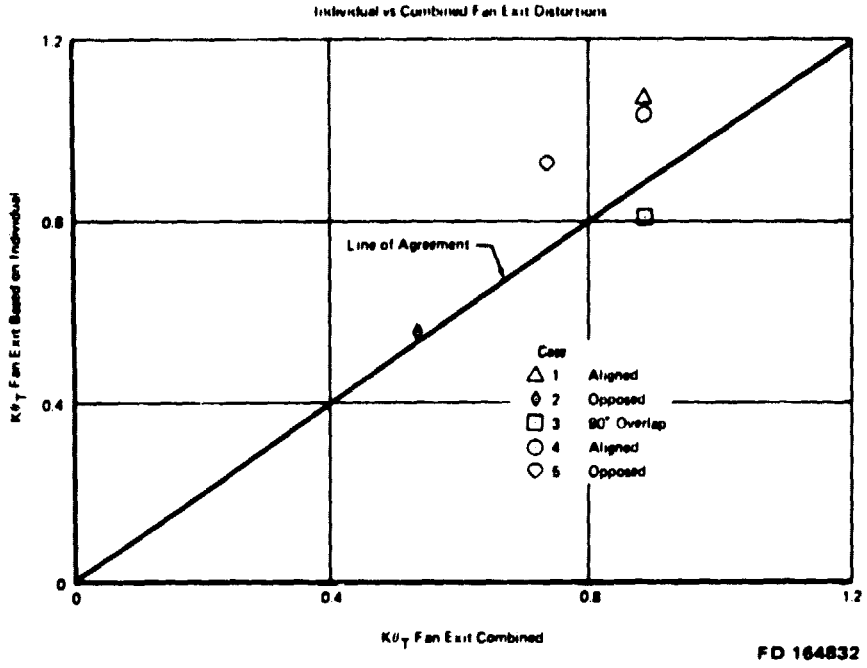

Figure 54. Combined Distortion Predictions: $K\theta_T$

XD11-8 STABILITY AUDIT

The distortion response parameters, defined for operation with individual and combined distortion, were used to predict the levels of distortion required to stall F100(3) engine XD11-8. This study was conducted as part of the pre-test planning for proposed NASA distortion tests using XD11-8. Stall distortion levels were predicted for each of the individual and combined distortion pattern types presented in figures 3 and 4. In addition, the stall-limiting component was identified for each case. This study demonstrated the usefulness of the analytical predictions in planning engine distortion tests. The pre-test predictions were used to define the required distortion generator capabilities and review the instrumentation and engine configuration requirements for the proposed tests.

The stability audit process consists of accounting for all the destabilizing factors that degrade engine stability margin. For the XD11-8 stability audit study, NASA data from past builds of this engine allowed definition of its particular operating line and undistorted surge line. Therefore, the primary destabilizing factor considered was the effect of the inlet distortion on engine surge line. High power (102% N1) audits used the predicted engine characteristics from the analysis of individual and combined distortions. However, for low power audits engine data was used for the pressure distortion characteristics since individual distortion analysis showed poor agreement between the model predictions and engine experience at this power. Low power temperature distortion characteristics were based on the model predictions because no data was available for this type of distortion.

Tables 3 and 4 present the results of the stability audits for engine XD11-8. For high power, audits showed that the fan was predicted to be the stall-limiting component when operating with inlet pressure distortion. Conversely, the high pressure compressor was the limiting component when operating with temperature distortion. Low power audits showed that the high compressor was predicted to be the limiting component for all cases. The predictions showed that high levels of distortion were required to stall the engine. These levels of distortion may exceed the capabilities of the test distortion generator. In fact, table 4 shows it is virtually impossible to generate a severe enough pressure distortion to stall XD-11 when the engine is matched on its nominal operating line. Therefore, engine rematch capability should be provided for the test program to permit raising both the fan and high compressor operating lines to reduce the available surge margin so that stalls can be induced during testing. This could be accomplished by providing a variable engine jet nozzle area for rematching the fan operating line and high pressure inbleed at the exit of the high compressor for rematching this component's operating line. In addition, the distortion profiles through the engine, generated by the model, should be used in locating instrumentation at both the fan inlet and exit, as well as defining the number of rotations of the distortion patterns required to establish the fan exit profiles.

Figures 55 and 56 present the results of the stability audits for operation with combined pressure and temperature distortion. Figure 55 shows the variation in temperature distortion for a fixed level of pressure distortion that will result in engine fan stall. As shown in the combined distortion analysis, the level of temperature distortion for a fixed pressure distortion that results in stall is a function of the relative orientation of the distortions. Similarly, figure 56 shows the variation in pressure distortion at a fixed temperature distortion required to stall the engine. These relationships can be used in planning the combined distortion portion of the XD11-8 test program.

Table 3. Predicted XD11 Stability Audits Individual Distortion — High Power

101.5% $N1/\sqrt{\theta_{T2}}$, WA $\sqrt{\theta_{T2}}$ /S_{T2} = 96.89 kg/sec (213.6 lb/sec)

Type	Extent	Stall Comp	$K\theta_p$ Stall	% Δ P/P Stall	$K\theta_T$ Stall	% ΔT/T Stall
Press	180	Fan	1.54	34	0	0
Press	90	Fan	1.54	48	0	0
Temp	180	HPC	0	0	1.34	30
Temp	90	HPC	0	0	1.34	42

Table 4. Predicted XD11 Stability Audits Individual Distortion — Low Power

70% $N1/\sqrt{\theta_{T2}}$, WA $\sqrt{\theta_{T2}}$ /δ_{T2} = 58.16 kg/sec (128.23 lb/sec)

Type	Extent	Stall Comp	$K\theta_p$ Stall	% Δ P/P Stall	$K\theta_T$ Stall	% ΔT/T Stall
Press	180	HPC	13.7	101.6	0	0
Press	90	HPC	13.7	143.6	0	0
Temp	180	HPC	0	0	2.54	22.7
Temp	90	HPC	0	0	2.54	32.0

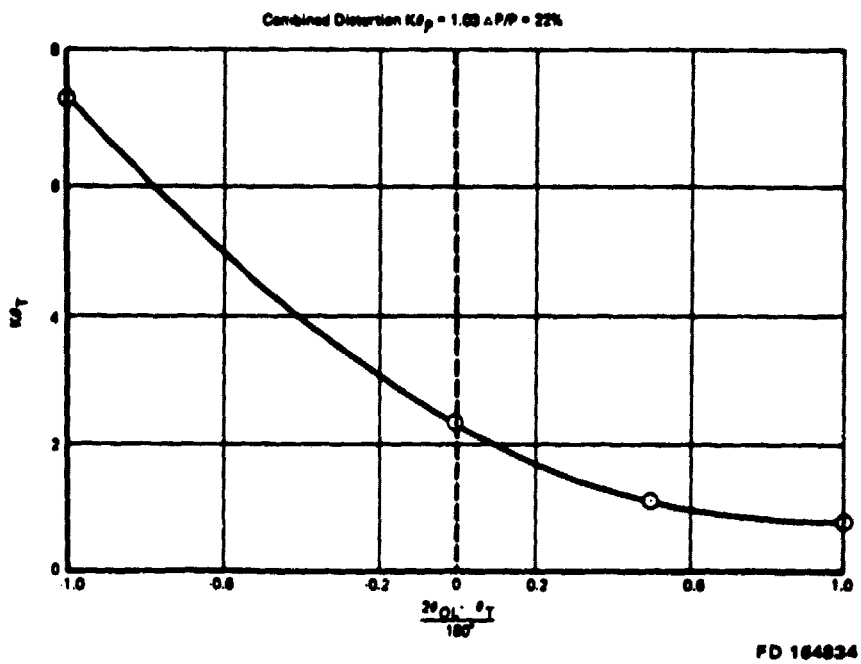

Figure 55. XD11 Stability Audit: $K\theta_p$ = 1.03, ΔP/P = 22%

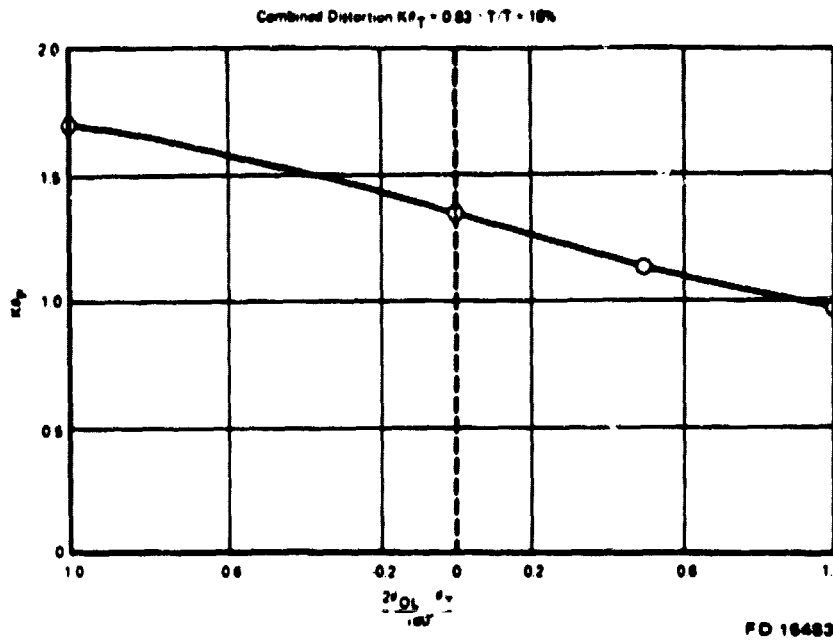

Figure 56. XD11 Stability Audit: $K\theta_T$ = 0.83, $\Delta T/T$ = 18%

CONCLUSIONS

1. The P&WA Multiple Segment Parallel Compressor Model provides a valuable tool which can be used to design improved engine stability tests.

2. The F100(3) version of the analytical model requires further development to provide reasonable low power predictions as current predictions show poor agreement with test results.

3. Significant discrepancies can occur between engine and rig stability test results if the rig exit static pressure field does not adequately simulate the engine environment.

4. Several pressure and temperature distortion extents, as well as amplitudes, should be tested to establish compressor component distortion response characteristics.

5. Several relative orientations of pressure and temperature distortions should be tested in combined distortion evaluations.

6. Prediction of combined distortion response characteristics from individual characteristics appears feasible. However, further study is required to define a general combined distortion analysis system when temperature distortion predominates.

7. The model predicts that F100(3) XD11-8 engine should encounter fan stalls with pressure distortion at high power, compressor stalls with temperature distortion at high power, and compressor stalls for all types of distortion at low power.

APPENDIX I
PRATT & WHITNEY AIRCRAFT GROUP F100 ENGINE DISTORTION DESCRIPTOR SYSTEM

A distortion descriptor system has been defined and continually refined during the F100 engine development and component improvements program. This system, was used in this program, is presented in tables 5 and 6 (pressure and temperature distortion descriptors, respectively).

Considering the exposure the F100 distortion descriptor system has had, only a brief description will be presented herein. The pressure distortion system (table 6) uses both fan and compressor pressure distortion indexes (KA_2 and KC_2, respectively). The fan pressure distortion index, KA_2, consists of a circumferential term, $K\theta$, a radial weighting factor, and a radial term, K_{ra2}. The compressor index, KC_2, represents the pressure distortion as measured at the fan face, which is considered to affect the compressor.

The F100 temperature distortion descriptor system (table 6) is quite similar to the pressure distortion system. Note, however, that the compressor temperature distortion index, K_{CT2}, has both a circumferential and radial term unlike the pressure distortion index, K_{C2}, where all radial pressure distortion is attenuated by the fan.

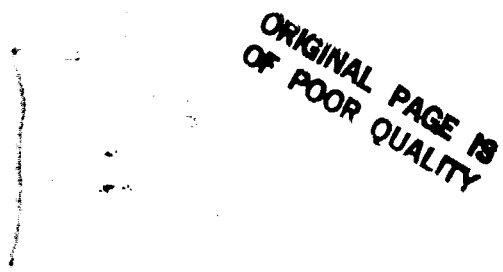

Table 5. P&WA/F100 Pressure Distortion Factors

Fan Pressure Distortion Factor, $K_{p2} = K_\theta + b\,K_{rn2}$

Fan Circumferential Pressure Distortion Factor, K_θ

$$K_\theta = \frac{\sum_{ring=1}^{J} \left[\left(\frac{A_N}{N^2}\right)_{max} \times \frac{1}{D_{ring}}\right]_{ring}}{(q/P_{t2})_{ref} \sum_{ring=1}^{J} \left[\frac{1}{D_{ring}}\right]}$$

where:

J = Number of rings (probes per leg)
D = Ring Diameter
$\left(\frac{q}{P_{t2}}\right)_{ref}$ = Reference value of engine face dynamic pressure

$$A_n = \sqrt{a_N^2 + b_N^2},\ N = 1,2,3,4$$

where:

$$a_N = \frac{\Delta\theta}{180} \sum_{k=1}^{K} \frac{P_{t2}/P_{t0}\ (k\Delta\theta)}{\bar{P}_{t2}/P_{t0}} \cos\ (Nk\Delta\theta)$$

$$b_N = \frac{\Delta\theta}{180} \sum_{k=1}^{K} \frac{P_{t2}/P_t\ (k\Delta\theta)}{\bar{P}_{t2}/P_{t0}} \sin\ (Nk\Delta\theta)$$

and

$P_{t2}/P_{t0}\ (k\Delta\theta)$ = Local recovery at angle, $k\Delta\theta$
$(\bar{P}_{t2}/P_{t0})$ = Face average recovery
K = Number of rake legs
$\Delta\theta$ = Angular distance between rake legs degrees

Fan Radial Pressure Distortion Term, $b\,K_{rn2}$

$$K_{rn2} = \frac{\sum_{ring=1}^{J} \left[\left(\frac{\Delta P_{t2}}{P_{t2}}\right)_{ring} \times \frac{1}{D''_{ring}}\right]}{(q/P_{t2})_{ref} \sum \frac{1}{D''_{ring}}}$$

with:

$$\left(\frac{\Delta P_{t2}}{\bar{P}_{t2}}\right)_{ring} = \left| \frac{(P^*_{t2}/P_{t0})}{\bar{P}_{t2}/P_{t0}} - \frac{P^*_{t2max}}{\bar{P}_{t2}} \right| \frac{\bar{P}_{t2}}{P^*_{t2max}}$$

Table 5. P&WA/F100 Pressure Distortion Factors (Continued)

where:

P^*_{t2}/P_{t_0} = ring average recovery

$\frac{P^*_{t2_{max}}}{P^-_{t2}}$ = reference radial profile, function of $(q/P_{t2})_{ref}$, CIVV

b = radial distortion weighting factor
P_{t_0} = Freestream total pressure
n = f (particular correlation) varies from 1 to 2.8
CIVV = fan inlet guide vane angle

High Compressor Pressure Distortion Factor, K_{c2}

$$K_{c2} = K_{\#_{splitter}} \frac{2\theta_{crit}}{\bar{\theta}}$$

where:

$K_{\#_{splitter}}$ is calculated in the same way as $K_{\#}$ but using values only for rings having diameters less than or equal to the splitter diameter. $D_{splitter}$, as defined below:

$$D_{splitter} = \sqrt{\alpha_s (OD^2 - ID^2) + ID^2}$$

OD = Outside diameter

ID = Inside diameter

α_s = splitter streamtube area ratio, function of $(q/P_{t2})_{ref}$

$\bar{\theta}$ = the greatest angular extent where $P_{t2}/P^*_{t2} < 1.0$. If there are two regions of low P_{t2}/P^*_{t2} separated by 25 deg or less, they are to be treated as one low-pressure region. The lower limit of $\bar{\theta}$ is to be 90 deg.

θ_{crit} = Circumferential extent of low pressure which is most detrimental to the compressor; assumed to be 90 deg for the F100/F401.

Table 6. P&WA F100 Temperature Distortion Factors

Fan Temperature Distortion Factor, $K_{A_1} = K_{\theta_1} + b_t K_{rat}$

Fan Circumferential Temperature Distortion Factor, K_θ

$$K_{\theta_1} = \frac{\sum_1^J \left\{ \frac{1}{T_{t_2}} \left[\frac{An}{N^2} \right]_{max} \frac{1}{D} \right\} \sqrt{\frac{180}{\theta_{hot}}}}{(0.1) \sum_1^J \frac{1}{D}}$$

where:

J = Number of Rings
D = Ring Diameter

$$\frac{An}{T_{t_2}} = \sqrt{\left(\frac{a_n}{T_{t_2}} \right)^2 + \left(\frac{b_n}{T_{t_2}} \right)^2}$$

$\frac{a_n}{T_{t_2}}$ = Nth coefficient of the sine term in a Fourier expansion of the T_t/T_{t_2} vs θ curve for one ring.

$\frac{b_n}{T_{t_2}}$ = Nth coefficient of the cosine term in a Fourier expansion of the T_t/T_{t_2} vs θ curve for one ring.

$\frac{1}{T_{t_2}} \left(\frac{A_n}{N^2} \right)_{max}$ = Maximum Value of $\left(\frac{A_n}{T_{t_2}} \right) /N^2$

N = Order of Fourier coefficient
θ_{hot} = Angle subtended by largest area of temperature in excess of the average temperature

Fan Radial Temperature Distortion Term, $b_t K_{rat}$

$$K_{rat} = \frac{\left\{ \sum_1^J \frac{\Delta T_{t_2}}{T_{t_2}} \frac{1}{D^2} \right\}}{(0.1) \sum_1^J \frac{1}{D^2}}$$

Table 6. P&WA F100 Temperature Distortion Factors (Continued)

where:

$$\frac{\Delta T_{t_2}}{\bar{T}_{t_2}} \frac{1}{D^2} = \left(\frac{\bar{T}_{t_2} - T_{t_2}^*}{\bar{T}_{t_2}} \right) \frac{1}{D^2}$$

$\left(\frac{\bar{T}_{t_2} - T_{t_2}^*}{\bar{T}_{t_2}} \right) \frac{1}{D^2}$ = Difference between the overall and ring average temperature, over the overall average temperature, multiplied by the weighting function $1/D^2$.

b_t = radial distortion weighing factor. High Compressor Temperature Distortion Factor, $K_{CT2} = K_{\#t\ splitter} + b_h K_{r\#t}$

HPC Circumferential Temperature Distortion Factor, $K_{\#t\ splitter}$

where:

$K_{\#t\ splitter}$ is calculated in the same way as $K_{\#b}$ but uses only the rings having diameters less than the splitter diameter, $D_{splitter}$.

$D_{splitter} = \sqrt{\alpha_s (OD^2 - ID^2) + ID^2}$

OD = Outside diameter

ID = Inside diameter

α_s = Splitter streamtube area ratio.

HPC Radial Temperature Distortion Term, $b_h K_{r\#t}$

where:

$K_{r\#t}$ is calculated as noted under fan radial distortion factor above.

b_h = radial distortion weighting factor.

APPENDIX II
DEFINITION OF MODEL INPUT PARAMETER VALUES

The Computer Code and User's Manual, Reference 1, provides detailed input instructions. The input card stream used for each case analyzed has been added to the program output; example cases for the fan and compressor are shown below. It is noted from the card stream that the compression system was divided into eighteen segments (NSEG=18), or 20 deg per segment. The fan analysis was performed for classical 180 and 90 deg patterns; thus, it is possible to use only two values of inlet total pressure and temperature (ISQ=0 and IK3=0). To analyze the high compressor, the pressure and temperature profiles were input on cards 6 and 7. Program calculated cross-flow fractions for the first solution were maintained for succeeding solutions (KBLEED = −1, ABCON = 1) to keep computing run times to a minimum. Also, if it became necessary to restart the compressor calculation, the cross-flow values from a previous run were specified (KBLEED = 1). The initial step size used in the exit static pressure backpressuring of the fan was set to one tenth of a percent (STPS=1.001). Program default values of the nondimensionalized unsteady rotor loss — lag were used (TAUND=1). To determine a fan stall point, a low value of total flow was specified (WCORR) and the calculations started at a flow rate above WCORR, such as the example case in which a five percent overflow was used (PCT2=0.05, PCT=0.05). The fan variable-guide vane was scheduled as a function of low rotor corrected speed (the schedule is a built-in feature of the program). The scheduling temperature sensors (TPLH1 and TPLH2) were specified to be at 150 and 210 deg. The analysis was performed for two fan corrected speeds (N1): 9842 and 6756, or 102 and 70% of design, respectively.

The average input pressure was $5.171 \times 10^4 n/m^2$ (7.5 psia) and average temperature for the 18% $\Delta T/T$, 180 deg case was 294.4°C (530°R). For subsequent temperature distortion cases, the low temperature region was fixed at 267.9°K (482.3°R). The inlet Reynolds Index was approximately 0.5. Bypass ratio for the fan was input. The bypass ratio used in Task I was determined by a user iteration in an attempt to match the high compressor on the nominal XD11 operating line with the predicted fan core exit corrected flow, speed, and profiles at the stall point. However, since it was felt the program was not intended to be an engine matching deck, considerable computing run time was saved in Task II by specifying a fixed bypass ratio and allowing the corrected flow rate into the HPC to be somewhat mismatched from the fan core exit. The fan was analyzed using run option (IOPT) of 4 (parallel compressor + particle swirl + unsteady rotor + upstream swirl).

To run the high compressor as a single spool, the predicted fan exit total pressure and temperature profiles were input (ISQ=1, IK3=1). The compressor variable vanes were set by a built-in vane schedule as a function of high rotor corrected speed. The inlet corrected speed used to read the schedule was input on card 3, columns 41 through 50. The Fortran logic to input the vane reading speed was built into the program; however, the User's Manual does not discuss this option. Vane scheduling corrected speed was calculated by the user based on the fan bypass exit temperature at 157 deg and a mechanical speed of 12,945 rpm for the high power match points and 10,475 for part power. The run option (IOPT) used for the compressor was 1 (parallel compressor + particle swirl + unsteady rotor).

```
INPUT LISTING                                    CARD COLUMN

         11111111112222222222333333333344444444445555555555666666666677777777778
12345678901234567890123456789012345678901234567890123456789012345678901234567890

CASE4 WITH PS INPUT    18   -1    0    1                                      -101

1.                              1.001                          1.        .05   .05
    1    2                                                150. 210. 157. 157.      1     1
200.       9842.                7.5        7.5        577.7      482.3      .52        4
1.0        1.0        1.0       1.0        1.0        1.0        1.0        1.0
1.0        1.0        1.0       1.0        1.0        1.0        1.0        1.0
1.0        1.0
```

```
INPUT LISTING                                    CARD COLUMN

         11111111112222222222333333333344444444445555555555666666666677777777778
12345678901234567890123456789012345678901234567890123456789012345678901234567890

F100 CASE4,HPC,.52BP   18   -1              1    1    1         0           -101

1.                              1.02                          1.
    3    4 1.        0.         0.        10666.     150. 210. 157. 157.
51.39      10567.    180.       23.976    23.976     778.43     778.43              1
10567.
23.38      23.25     23.09      22.81     23.17      23.67      23.93      24.27
24.60      24.86     25.03      25.13     25.21      24.15      24.02      23.85
23.66      23.5
831.1      831.7     833.6      836.9     826.5      782.2      731.5      716.3
716.2      716.9     718.3      719.8     721.2      742.7      797.2      827.0
831.6      831.1
```

LIST OF SYMBOLS

IRS	Blade Row Index
$K\theta_P$	F100 Circumferential Pressure Distortion Factor
$K\theta_T$	F100 Circumferential Temperature Distortion Factor
$K\theta_{fan}$	F100 Circumferential Distortion Factor for Fan Inlet Conditions
$\Delta P/P$	(PTMAX – PTMIN)/PTAVG
PS	Static Pressure
PSI	Normalized Pressure Rise
PTL	Local Total Pressure
TT_2	Local Total Temperature
PTMAX	Highest Total Pressure in Distortion Pattern
PTMIN	Lowest Total Pressure in Distortion Pattern
PTAVG	Average Total Pressure
$\Delta T/T$	(TTMAX – TTMIN)/TTAVG
TTMAX	Highest Total Temperature in Distortion Pattern
TTMIN	Lowest Total Temperature in Distortion Pattern
TTAVG	Average Total Temperature
PTexit	Fan Exit Average Total Pressure
PTinlet	Fan Inlet Average Total Pressure
U	Wheel Speed — FPS
WAC	Corrected Airflow
Wat	Total Inlet Airflow lb/sec
θT2	Inlet TTAVG/518.7
δT2	Inlet PTAVG/14.7
θ_{OL}	Angular Overlap of Pressure and Temperature Distortion
θ_T	Angular Extent of Temperature Distortion
XND	Design Speed — rpm
XNC	Local Corrected Rotor Speed

REFERENCES

1. Mazzawy, R. S., D. A. Fulkerson, D. E. Haddad and T. A. Clark, "F100(3) Parallel Compressor Computer Code and User's Manual Final Report," NASA CR-135388, May 1978.

2. Mazzawy, R. S. "Multiple Segment Parallel Compressor Model for Circumferential Flow Distortion," ASME *Journal of Engineering for Power*, Vol. 99, No. 2, April 1977.

3. Braithwaite, W. M., E. J. Graber, Jr., and C. M. Mehalic, "The Effect of Inlet Temperature and Pressure Distortion on Turbojet Performance," AIAA Paper No. 73-1316.

4. Mazzawy, R. S. and G. A. Banks, "Circumferential Distortion Modeling of the TF30-P-3 Compression System," NASA CR-135124, January 1977.

5. Greitzer, E. M., R. S. Mazzawy, D. A. Fulkerson, "Flow Field Coupling Between Compression System Components in Asymmetric Flow," Transaction of the ASME, January 1978.